

**MODELING OF GRASSED LEVEE EROSION BY  
IRREGULAR WAVE ACTION**

BY

HEATHER WEITZNER AND NOBUHISA KOBAYASHI

RESEARCH REPORT NO. CACR-14-01  
2014



**CENTER FOR APPLIED COASTAL RESEARCH**

Ocean Engineering Laboratory  
University of Delaware  
Newark, Delaware 19716

## **ACKNOWLEDGMENTS**

This study was partially supported by the U.S. Army Corps of Engineers under contract No. W911XK-13-P-0065 and by the EU THESEUS Project.

## TABLE OF CONTENTS

LIST OF FIGURES.....	iii
ABSTRACT.....	v
1 INTRODUCTION.....	1
2 LEVEE EROSION MODEL.....	4
3 TURF FAILURE UNDER STEADY FLOW.....	13
4 EROSION OF SEAWARD GRASSED SLOPE.....	16
5 EROSION OF SEAWARD CLAY SLOPE.....	30
6 EROSION OF LANDWARD GRASSED SLOPE.....	35
7 SUMMARY AND CONCLUSIONS.....	43
REFERENCES.....	45

## LIST OF FIGURES

Figure 1	Definition sketch for levee erosion model .....	4
Figure 2	Definition sketch of grass cover (Muijs 1999) .....	6
Figure 3	Resistance force parameter $R$ as a function of vertical erosion depth $E$ ...	8
Figure 4	Limiting velocity $U_L$ as a function of steady flow duration $t_d$ .....	14
Figure 5	Classification of grass according to the Dutch guidelines for primary defenses as presented by Hoffmans et al. (2008) .....	15
Figure 6	Computed erosion depth increase with time $t$ for test 6.....	17
Figure 7	Computed hydrodynamics associated with test 6.....	18
Figure 8	Measured and computed erosion rates on seaward grass cover for test 6 .....	20
Figure 9	Computed erosion depth increase with time $t$ for test 7.....	21
Figure 10	Computed hydrodynamics associated with test 7 .....	22
Figure 11	Measured and computed erosion rates on seaward grass cover for test 7 .....	23
Figure 12	Computed erosion depth increase with time $t$ for test 6H with poor grass patch .....	25
Figure 13	Computed hydrodynamics associated with test 6H .....	26
Figure 14	Computed erosion depth increase with time $t$ for test 7H with poor grass patch .....	28
Figure 15	Computed hydrodynamics associated with test 7H.....	29
Figure 16	Measured and computed profile evolutions of seaward clay slope .....	31
Figure 17	Computed hydrodynamics on seaward clay slope .....	33

Figure 18	Increase of measured and computed eroded areas with time $t$ for seaward clay slope .....	34
Figure 19	Increase of computed wave overtopping rate $q_o$ with still water level $S$ for test VI.....	36
Figure 20	Computed erosion depth increase with time $t$ for test VI with poor grass patch .....	37
Figure 21	Computed maximum erosion depth $E_{\max}$ at slope transition of good grass cover as a function of $q_o$ and $t$ .....	39
Figure 22	Computed maximum erosion depth $E_{\max}$ at slope transition of poor grass cover as a function of $q_o$ and $t$ .....	40
Figure 23	Computed maximum erosion depth $E_{\max}$ at slope transition of landward clay slope as a function of $q_o$ and $t$ .....	41

## **ABSTRACT**

A levee erosion model is developed to predict the temporal and cross-shore variations of vertical erosion depth under irregular wave action. The product of the erosion rate and the turf resistance force is related to the wave energy dissipation rates due to wave breaking and bottom friction. The turf resistance force is expressed using the turf thickness and the surface and underneath resistance parameters. The empirical parameters are calibrated using available data. The calibrated model is shown to reproduce the relation between the limiting velocity and steady flow duration, the erosion rate on a seaward grassed slope, and the eroded profile evolution of a seaward clay slope. The levee erosion model is also compared with field and laboratory tests for erosion on the landward slope caused by wave overtopping. It is found to be difficult to reproduce the observed erosion initiation and progression because of the wide variations of the grass cover and clay resistance. The turf resistance parameters will need to be calibrated for specific levees.

## **Chapter 1**

### **INTRODUCTION**

Levees (dikes) have been constructed to protect some coastal areas against flooding by the combined action of storm surge and wind waves. The prediction of levee erosion is essential for the risk-based design of the levee. A number of large-scale laboratory experiments were conducted to quantify the erodibility and resilience of seaward levee slopes (e.g., Klein Breteler et al. 2012). Erosion of landward levee slopes has been investigated on actual levees using the Wave Overtopping Simulator (e.g., van der Meer et al. 2010) which mimics irregular wave overtopping events for the specified wave overtopping rate. The separate studies for the seaward and landward levee slopes have not been synthesized probably because of the different hydrodynamics involved on the seaward and landward slopes. Erosion on the seaward slope is caused by irregular breaking waves and wave uprush and downrush in the swash zone. Erosion on the landward slope is caused by intermittent wave overtopping of the levee whose crest elevation is normally designed to be higher than the design storm tide to avoid overflow. The similarity of the hydrodynamics involved in levee erosion and dune erosion is utilized herein to develop a numerical model for predicting the cross-shore and temporal variations of the erosion depth on the entire levee.

The cross-shore numerical model, CSHORE, has been shown to be capable of predicting beach erosion by irregular breaking waves (Kobayashi et al. 2008), berm and dune erosion by the combined action of storm surge and waves (Kobayashi et al.

2009), and dune overwash by intermittent wave overtopping (Kobayashi et al. 2010b). The sand transport formulas used in CSHORE are not applicable to the grass cover and underneath cohesive sediment of the levee. A levee erosion model is proposed by generalizing the work-based formula by Dean et al. (2010). The rate of work for levee erosion is expressed as the product of the vertical erosion rate and the resistance force of the grass and cohesive sediment. This rate of work is related to the energy dissipation rates due to wave breaking and bottom friction predicted by the hydrodynamic model in CSHORE. The resistance force is assumed to decrease downwind linearly in the turf zone with roots and be represented by the turf thickness and the surface and underneath resistance forces. The three parameters for the grass and soil characteristics are calibrated using available data.

The paper is organized as follows. First, the levee erosion model is presented along with the simple parameterization of the sward, roots and substrate of the grass cover protecting the levee against irregular wave action. Second, the grass cover parameters are estimated using the empirical curves by Hewlett et al. (1987) between the limiting velocity and steady flow duration for different grass covers. The grass cover failure is assumed to occur when the erosion depth exceeds the turf thickness. Third, the levee erosion model is compared with the large-scale experiment by Smith et al. (1994) who measured the erosion depth of the grass cover under irregular breaking waves on the seaward levee slope. The breaking wave efficiency of the levee erosion is calibrated to be much smaller than the efficiency of breaking waves in suspending sand grains on beaches. Fourth, the large-scale experiment by Wolters et al. (2008) is used to examine whether the levee erosion model with no grass cover can predict the measured erosion profiles of the seaward clay slope. Fifth, the levee

erosion model is compared with the field experiment by Steendam et al. (2010) who investigated the grass cover erosion on the landward slope for different wave overtopping rates. Finally, the findings of this study are summarized.

## Chapter 2

### LEVEE EROSION MODEL

The cross-shore model CSHORE (Kobayashi et al. 2010b) is applied to an emerged levee as depicted in Figure 1.

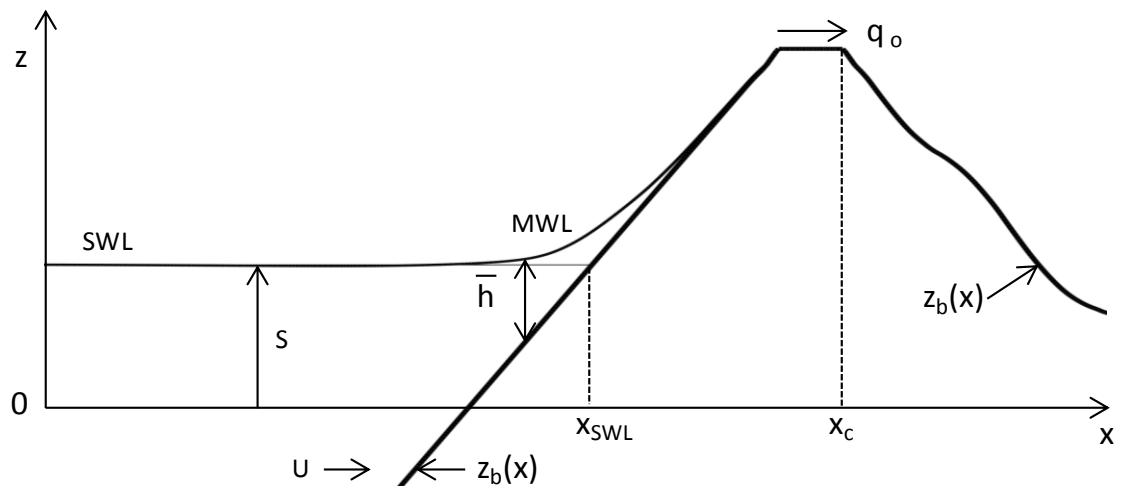


Figure 1 Definition sketch for levee erosion model

Alongshore uniformity and normally incident waves are assumed. The cross-shore coordinate  $x$  is positive onshore with  $x = 0$  at the toe of the levee. The vertical coordinate  $z$  is positive upward with  $z = 0$  at the datum. The still water level (SWL) is located at the elevation of  $z = S$  with  $S =$  storm tide. For comparisons with laboratory data with constant  $S$ , the datum is taken at SWL and  $S = 0$ . The hydrodynamic model in CSHORE predicts the mean ( $\bar{\eta}$  and  $\bar{U}$ ) and standard deviation ( $\sigma_{\eta}$  and  $\sigma_U$ ) of the free

surface elevation  $\eta$  and depth-averaged cross-shore velocity  $U$  where the overbar denotes time averaging. The mean water level (MWL) is located at  $z = (\bar{\eta} + S)$ . The mean water depth  $\bar{h}$  is given by  $\bar{h} = (\bar{\eta} + S - z_b)$  with  $z_b$  = levee surface elevation varying with  $x$ . The intermittently wet and dry zone in CSHORE is assumed to occur landward of the still water shoreline located at  $x = x_{\text{SWL}}$ . The wave overtopping rate  $q_o$  is estimated as the time-averaged volume flux at the most landward location  $x_c$  of the horizontal levee crest. The levee surface elevation  $z_b$  decreases slowly with time  $t$  because of erosion by irregular wave action. The eroded material is assumed to be transported out of the computation domain in the present levee erosion model.

The hydrodynamic model in CSHORE is coupled with the levee erosion model developed in this study in light of earlier studies. Hoffmans et al. (2008) analyzed vertical forces acting on a turf element. The turf has a high root density and the root structure binds clay aggregates together. The turf element model is appealing physically but requires the detailed root and soil characteristics. Below is a physical depiction of the grass cover and turf, as detailed by Hoffmans et al. (2008) on the basis of Muijs (1999).

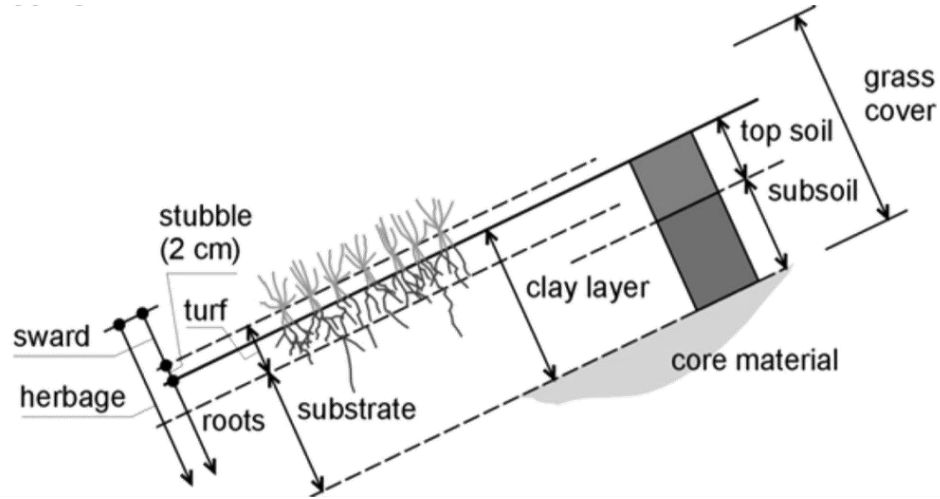


Figure 2 Definition sketch of grass cover (Muijs 1999)

Dean et al. (2010) proposed erosion indices based on excess work for the landward grassed slope. Dean and van Ledden (2010) applied the erosion indices to explain the failure of one levee and the survival of another levee in the New Orleans area during 2005 Hurricane Katrina. These indices do not indicate the degree of damage. van der Meer et al. (2010) proposed cumulative hydraulic load indices for different damage levels using their Wave Overtopping Simulator data. The present model attempts to predict the temporal and cross-shore variations of the vertical erosion depth  $E$  defined as

$$E(t, x) = [z_b(t=0, x) - z_b(t, x)] \geq 0 \quad (1)$$

where the initial levee profile  $z_b(x)$  at  $t = 0$  is input to the numerical model. The eroded levee profile  $z_b(t, x)$  at given time  $t > 0$  can be predicted using Equation 1 if  $E(t, x)$  is predictable. The prediction of the eroded levee profile becomes similar to the

prediction of the beach profile evolution using CSHORE (e.g., Kobayashi et al. 2008) except that no deposition is allowed in this levee erosion model.

The resistance force of the turf per unit horizontal area is denoted as  $(\rho R)$  with  $\rho$  = fluid density and  $R$  = resistance force divided by  $\rho$  so that its unit is  $m^2/s^2$ . The rate of erosion work is expressed as the product of the resistance force and the vertical erosion rate

$$\rho R \frac{\partial E}{\partial t} = D \quad \text{with } E = 0 \quad \text{at } t = 0 \quad (2)$$

where  $D$  = energy dissipation rate per unit horizontal area corresponding to the rate of erosion work. Subsequently,  $D$  is related to the rate of fluid energy dissipation. The vertical distribution of the turf resistance depends on the detailed root and soil structures. The simple distribution of  $R$  shown in Figure 3 is adopted and  $R$  is expressed as

$$R = R_0 - (R_0 - R_d) \frac{E}{d} \quad \text{for } 0 \leq E \leq d \quad (3)$$

$$R = R_d \quad \text{for } d \leq E \quad (4)$$

where  $d$  = turf thickness; and  $R_0$  and  $R_d$  = turf surface and underneath resistance parameters, respectively. The substrate resistance is assumed to be invariant vertically and represented by  $R_d$ . Equation 4 will need to be modified for a levee with sand core (e.g., Klein Breteler et al. 2012). The grass cover is characterized by the three parameters  $d$ ,  $R_0$  and  $R_d$  which are allowed to vary spatially.

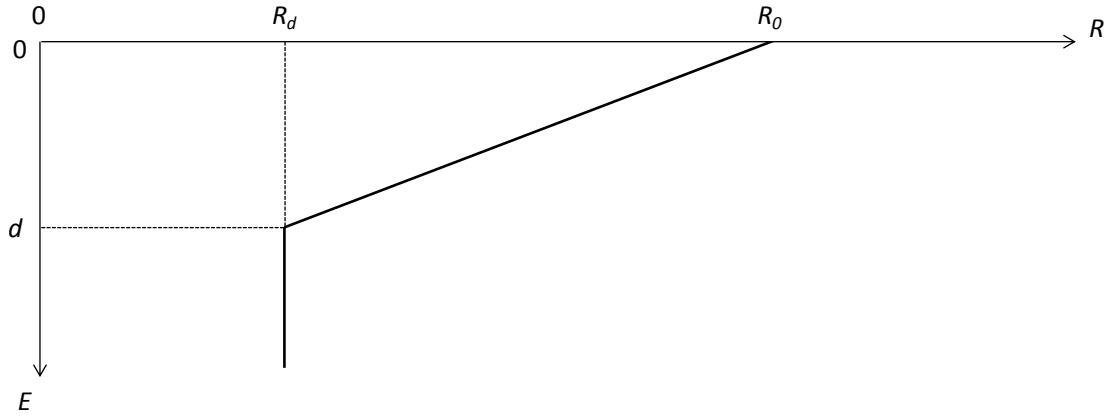


Figure 3 Resistance force parameter  $R$  as a function of vertical erosion depth  $E$

Equation 2 can be integrated analytically for  $R$  given by Equations 3 and 4.

The temporal variation of  $D$  in Equation 2 is arbitrary and the temporal variation of the local erosion depth is given by

$$E(t) = \frac{dR_0}{R_0 - R_d} \left\{ 1 - \left[ 1 - \frac{2(R_0 - R_d)}{dR_0^2} F(t) \right]^{0.5} \right\} \quad \text{for } 0 \leq t \leq t_d \quad (5)$$

$$E(t) = \frac{F(t)}{R_d} - \frac{d(R_0 - R_d)}{2R_d} \quad \text{for } t_d \leq t \quad (6)$$

with

$$F(t) = \int_0^t \frac{D}{\rho} dt \quad ; \quad F(t_d) = \frac{d(R_0 + R_d)}{2} \quad (7)$$

where  $E(t_d) = d$  and  $t_d$  is the duration required to erode the turf of thickness  $d$ . For the case of no grass cover ( $d = 0$ ),  $t_d = 0$  and Equation 6 yields  $E(t) = F(t)/R_d$ .

For the case of very small erosion ( $E/d \ll 1$ ), Equation 5 can be approximated as  $E(t) \cong (F(t)/R_0)$  and the erosion depth is inversely proportional to  $R_0$ .

In the wet zone where water is present always, the dissipation rate  $D$  is assumed to be given by

$$D = (e_B D_B + e_f D_f) G_s(S_b) \quad ; \quad S_b = \frac{\partial z_b}{\partial x} \quad (8)$$

where  $D_B$  and  $D_f$  = energy dissipation rates per unit horizontal area due to wave breaking and bottom friction, respectively;  $e_B$  and  $e_f$  = efficiencies for  $D_B$  and  $D_f$ , respectively; and  $G_s$  = function of the bottom slope  $S_b$  introduced to increase erosion on the steep levee slope. The equations for  $D_B$  and  $D_f$  given by Kobayashi et al. (2010b) include the breaker ratio parameter  $\gamma$  and the bottom friction factor  $f_b$ . Kobayashi et al. (2013) compared CSHORE with a large number of irregular wave runup and overtopping of fixed levees using  $\gamma = 0.7$  and  $f_b = 0.02$ . These values are adopted in the following. The efficiencies used for sand suspension are  $e_B = 0.005$  and  $e_f = 0.01$  (Kobayashi et al. 2008). The calibrated value of  $e_B$  for erosion of seaward levee slopes is  $e_B = 0.0002$  as will be explained later. Levee erosion by breaking waves is much less efficient than sand suspension by breaking waves. The value of  $e_f = 0.01$  is adopted because the bottom friction acts more continuously than the intermittent breaking wave action. The bottom slope function  $G_s$  introduced by Kobayashi et al. (2008) for bed load transport is modified as

$$G_s(S_b) = \frac{S_c}{S_c - |S_b|} \quad \text{for} \quad |S_b| < S_c \quad (9)$$

where  $S_c$  = upper limit of the eroded clay slope. The calibrated value for a seaward clay slope is  $S_c = 1.2$  as will be shown later. Equation 9 is applicable to positive (upward) and negative (downward) slopes. The value of  $G_s$  increases from 1.0 for  $S_b = 0$  with the increase of  $|S_b|$  and the upper limit of  $G_s = 10$  is imposed as is the case with  $G_s$  for bed load transport.

In the intermittently wet and dry zone  $x \geq x_{\text{SWL}}$  in Figure 1, no wave breaking is assumed to occur and  $D$  is given by

$$D = e_d D_f G_s(S_b) \quad \text{for } x \geq x_{\text{SWL}} \quad (10)$$

where the efficiency  $e_d$  is chosen so that the values of  $D$  given by Equations 8 and 10 are the same at  $x = x_{\text{SWL}}$  for the smooth transition between the two zones as explained by Kobayashi et al. (2010a). The energy dissipation rate  $D_f$  due to bottom friction is expressed as

$$D_f = \frac{1}{2} \rho f_b \int_0^\infty |U|^3 f(h) dh \quad (11)$$

with

$$U = \alpha \sqrt{gh} + U_s \quad ; \quad f(h) = \frac{P_w^2}{h} \exp\left(-P_w \frac{h}{h}\right) \quad (12)$$

where  $U$  = instantaneous horizontal velocity;  $h$  = instantaneous water depth;  $f(h)$  = probability density function of  $h$  in the wet and dry zone;  $\alpha$  = constant taken as  $\alpha = 2$ ;  $g$  = gravitational acceleration;  $U_s$  = steady velocity included to account for offshore return flow on the seaward slope and crest and the downward velocity increase on the

landward slope;  $\bar{h}$  = mean water depth during the wet duration of  $h > 0$ ; and  $P_w$  = wet probability of  $h > 0$ . The dry probability of  $h = 0$  is equal to  $(1 - P_w)$ . The cross-shore variations of  $\bar{h}$ ,  $P_w$  and  $U_s$  are predicted using the hydrodynamic model in the wet and dry zone (Kobayashi et al. 2010a; 2010b) which was shown to predict the depth and velocity measurements by van Gent (2002) mostly within a factor of 2. Substitution of Equation 12 into Equation 11 yields

$$D_f = \frac{1}{2} \rho f_b \frac{\alpha^3 (g \bar{h})^{1.5}}{\sqrt{P_w}} G_d(r) \quad ; \quad r = \frac{3\sqrt{\pi}}{4} \frac{U_s \bar{h}}{q_o - U_s \bar{h}} \quad (13)$$

with

$$G_d(r) = \frac{3\sqrt{\pi}}{4} + 3r + \frac{3\sqrt{\pi}}{2} r^2 + r^3 \quad \text{for } r \geq 0 \quad (14)$$

$$G_d(r) = \frac{3\sqrt{\pi}}{4} (1 + 2r^2) [1 - 2\text{erf}(r)] - 3r - r^3 + (16r^3 + 9r) \exp(-r^2) \quad \text{for } r < 0 \quad (15)$$

where  $\text{erf}$  = error function and the wave overtopping rate  $q_o$  is the time-averaged volume flux at  $x = x_c$  in Figure 1.

The computation procedure is as follows. The initial levee profile and the cross-shore variations of  $d$ ,  $R_0$  and  $R_d$  in Equations 3 and 4 are specified at time  $t = 0$  before the time-marching computation. The time series of the still water level  $S$  and the spectral significant wave height  $H_{m0}$  and the peak period  $T_p$  at the seaward boundary  $x = 0$  are also specified where  $\bar{\eta} = 0$  at  $x = 0$  is assumed at the toe of the levee. The hydrodynamic model in CSHORE is used to compute the dissipation rate  $D$  given by Equations 8 and 10. The time step  $\Delta t$  for the integration of  $F(t)$  in Equation 7 is chosen as  $\Delta t = \rho \delta / (D/R_d)_m$  in light of Equation 2 where  $\delta =$

allowable erosion depth increment and  $(D/R_d)_m =$  maximum computed value of  $(D/R_d)$ . The following computations for large-scale and prototype levees are made using  $\delta = 5$  cm. The erosion depth  $E$  is computed using Equations 5 and 6. The levee profile  $z_b$  at the next time level is obtained using Equation 1. This time-marching computation is repeated until the end of a levee erosion test. The computation time is of the order of  $10^{-3}$  of the test duration. The computational efficiency is essential for the development of the levee erosion model which is empirical and requires the calibration of several parameters.

### Chapter 3

#### TURF FAILURE UNDER STEADY FLOW

For steady flow on a gentle slope, Equation 8 can be simplified as  $D = e_f D_f$  with  $D_f = 0.5\rho f_b U^3$  where  $U$  = steady flow velocity. The function  $F(t)$  in Equation 7 reduces to  $F(t) = 0.5e_f f_b U^3 t$ . The failure of a turf may be assumed to occur when the erosion depth  $E$  becomes equal to the turf thickness  $d$ . This failure condition corresponds to the equation of  $F(t_d)$  in Equation 7 which is used to obtain the relation between the flow duration  $t_d$  and corresponding limiting velocity  $U_L$

$$U_L^3 t_d = d(R_0 + R_d) / (e_f f_b) \quad (16)$$

Equation 16 indicates  $U_L^3 t_d = \text{constant}$  if the turf parameters  $d$ ,  $R_0$  and  $R_d$  are constant. Figure 4 shows the relation of  $U_L^3 t_d = C$  fitted to the curves for the good, average, and poor grass covers given by Hewlett et al. (1987). The fitted values of  $C$  are in the range of  $10^5$  to  $6 \times 10^5 \text{ m}^3/\text{s}^2$ . Dean et al. (2010) fitted their excess work relation with two constants and obtained better fits. Young and Hassan (2006) compared the curves in Hewlett et al. (1987) with other data and discussed the crude nature of the curves in Hewlett et al. (1987).

Grass Cover	Data	Fitted	$C \times 10^5 \text{ m}^3/\text{s}^2$
Good	○	—	6
Average	●	⋯	3
Poor	X	—	1

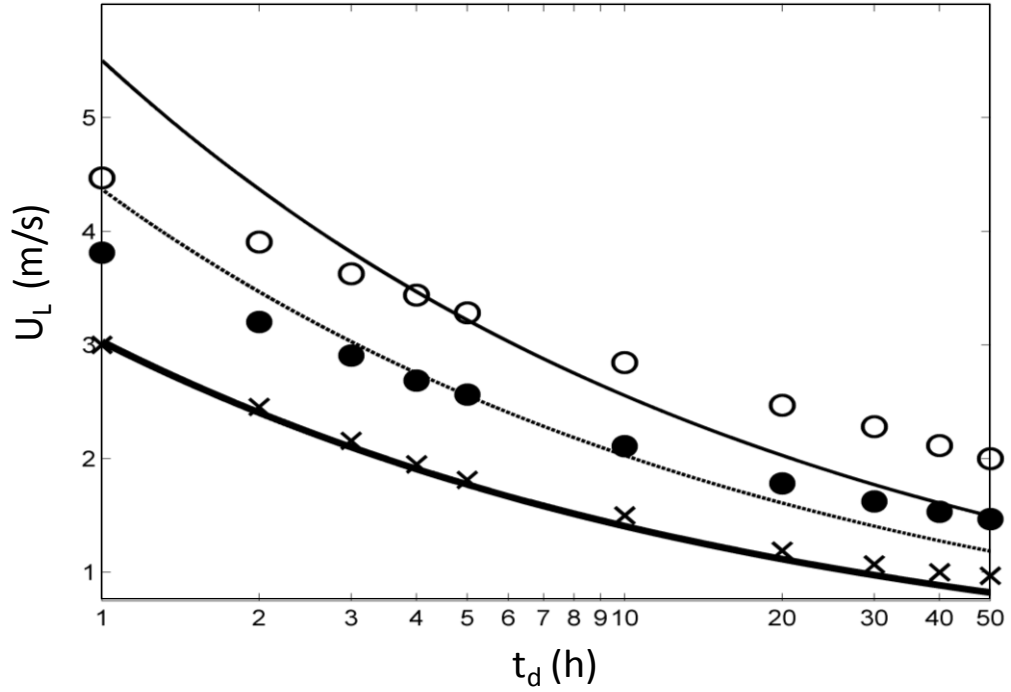


Figure 4 Limiting velocity  $U_L$  as a function of steady flow duration  $t_d$

A crude estimate of  $(R_0 + R_d)$  is obtained using Equation 16 and the fitted values of  $C$ . A typical value of the turf thickness  $d$  is taken at  $d = 0.1$  m on the basis of the vertical decrease of the number of roots per unit surface area plotted by Hoffmans et al. (2008) as reproduced in Figure 5 for convenience.

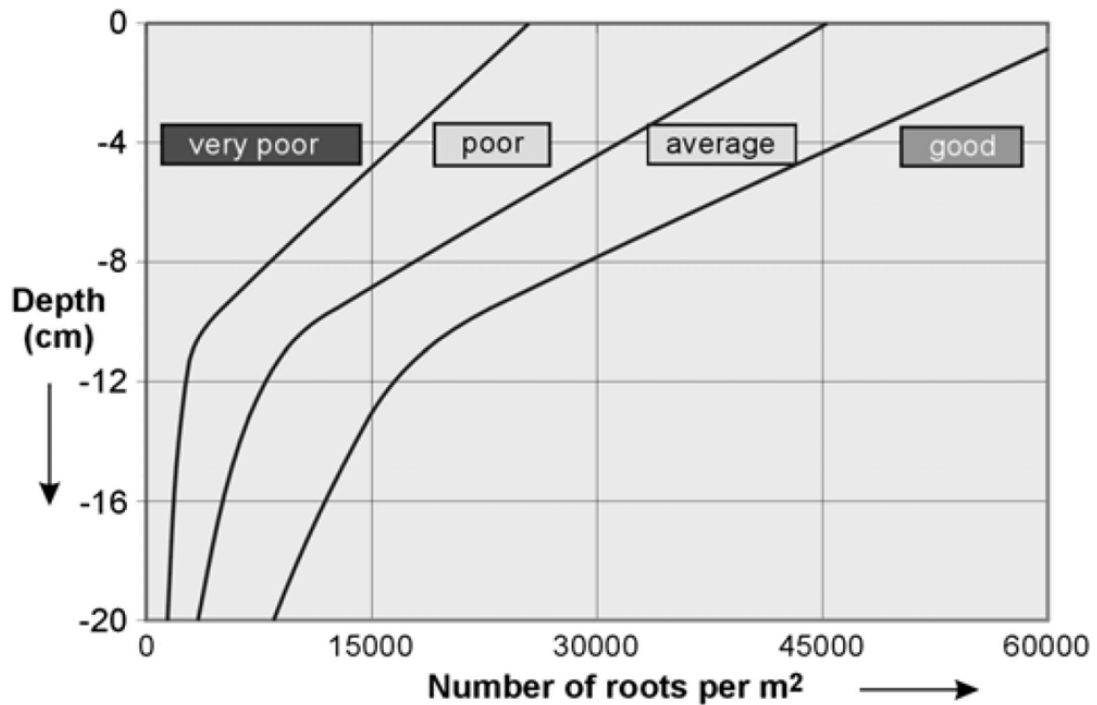


Figure 5 Classification of grass according to the Dutch guidelines for primary defenses as presented by Hoffmans et al. (2008)

The efficiency  $e_f$  and the bottom friction factor  $f_b$  are estimated as  $e_f = 0.01$  and  $f_b = 0.02$  as explained below Equation 8, for  $C = 10^5$  to  $6 \times 10^5 \text{ m}^3/\text{s}^2$ ,  $(R_0 + R_d) = 200$  to  $1200 \text{ m}^2/\text{s}^2$ . The turf surface resistance parameter  $R_0$  is expected to be much larger than the underneath resistance parameter  $R_d$ . The erosion experiment of a seaward clay slope by Wolters et al. (2008) is used to calibrate  $R_d = 10 \text{ m}^2/\text{s}^2$  as will be shown later. In the following, a typical value of  $R_0$  is taken as  $R_0 = 1,000 \text{ m}^2/\text{s}^2$  for a good grass cover and  $R_0 = 200 \text{ m}^2/\text{s}^2$  for a poor grass cover. These estimates may not be accurate but indicate the large variation of the turf and substrate resistance against erosion.

## Chapter 4

### EROSION OF SEAWARD GRASSED SLOPE

Smith et al. (1994) excavated 16 blocks from a section of an existing sea levee in the Netherlands. The length, width, and thickness of each block were 2.5 m, 2.5 m, and 1.0 m, respectively. The blocks were transported to reconstruct the levee section in a large wave flume. The grass cover and clay substrate layer of 1-m thickness was placed on the seaward and landward slopes of 1/4 and 1/2.5, respectively. The grass cover was inspected in detail and found to be good. The width of the concrete crest was 2 m and the crest height was 7 m above the flume horizontal bottom. The levee erosion model is compared with the erosion tests 6 and 7. The water depth at the levee toe was 4.8 and 3.5 m for tests 6 and 7, respectively. The significant wave height  $H_s$  and the peak period  $T_p$  were 1.4 m and 4.7 s for test 6, respectively. For test 7,  $H_s = 0.75$  m and  $T_p = 3.4$  s. The test duration was 11 h for test 6 and 20 h for test 7. For the following computations, the spectral significant wave height  $H_{mo}$  is assumed to be the same as  $H_s$  and given by  $H_{mo} = 4\sigma_\eta$ . The good grass cover is represented by  $d = 0.1$  m,  $R_0 = 1,000$  m<sup>2</sup>/s<sup>2</sup> and  $R_d = 10$  m<sup>2</sup>/s<sup>2</sup> in Figure 3. The value of  $R_0$  is increased to  $R_0 = 10,000$  m<sup>2</sup>/s<sup>2</sup> for the concrete sections of the constructed levee. These values should be regarded as order-of-magnitude estimates.

For test 6, the grass cover inspection and profile survey were performed every hour. The erosion depth  $E$  with  $E = 0$  at time  $t = 0$  is computed and plotted in Figure 6 as a function of  $x$  at  $t = 1, 2, \dots, 11$  h. The maximum erosion depth for test 6 is on

the order of several centimeters. Although the erosion depth increases with time, it does not exceed the turf thickness  $d$ .

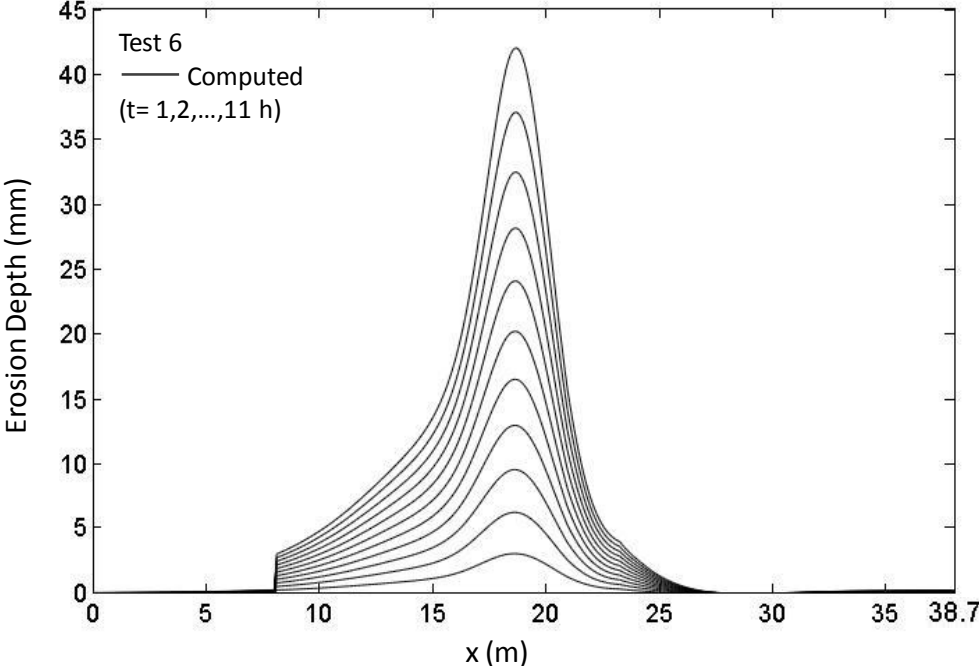


Figure 6 Computed erosion depth increase with time  $t$  for test 6

The computed cross-shore variations of  $\bar{\eta}$ ,  $\sigma_{\eta}$ ,  $\bar{U}$ ,  $\sigma_U$  and  $P_w$  vary very little with time because of the small erosion and constant wave conditions, as shown in Figure 7. As a result, the temporal changes of  $R$  and  $D$  in Equation 2 are small and the value of  $\frac{\partial E}{\partial t}$  changes little with time. The computed cross-shore variations of the erosion rate ( $E/t$ ) at  $t = 1, 2, \dots, 11$  h are shown along with the experimental levee section in Figure 8.

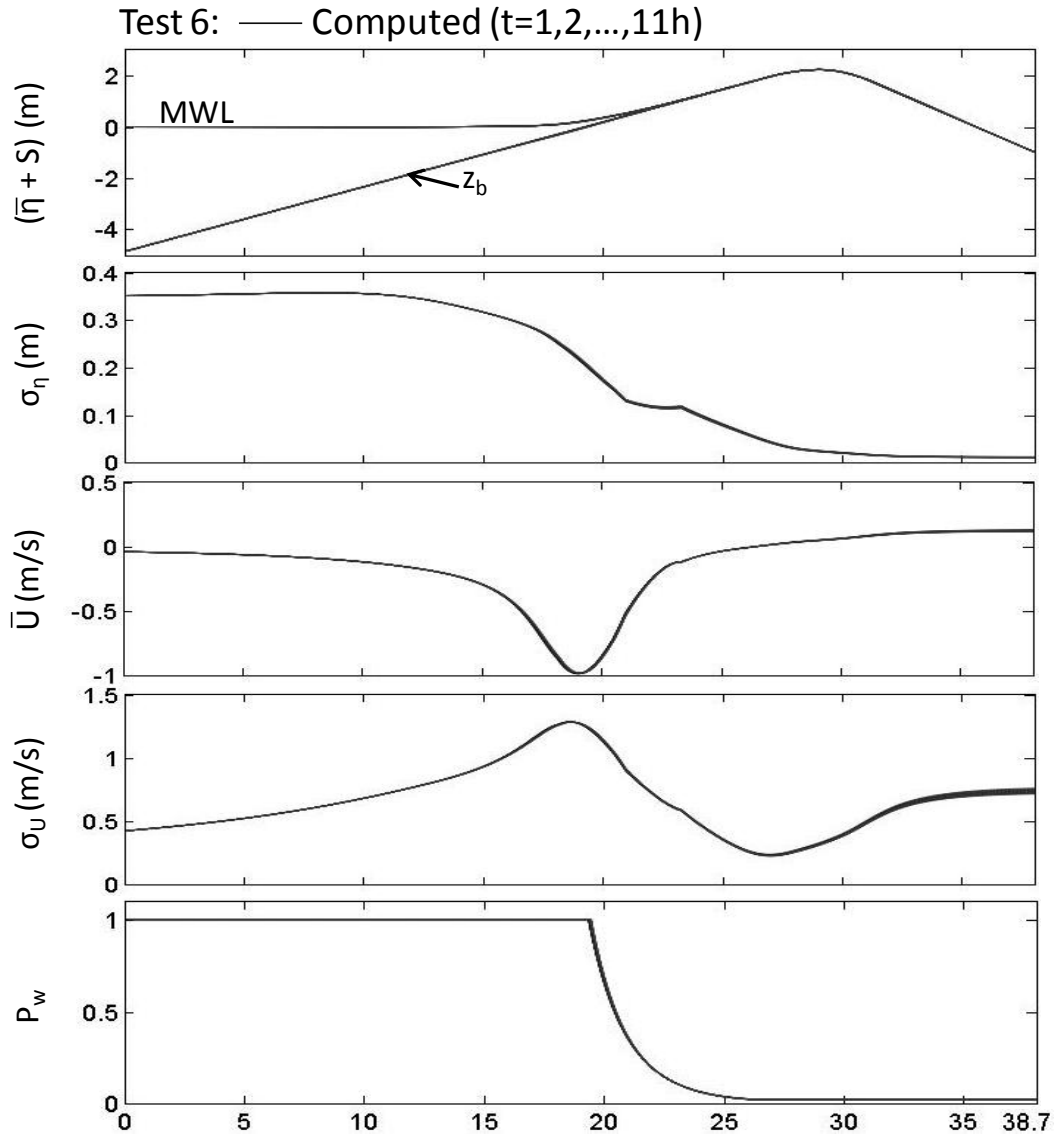


Figure 7 Computed hydrodynamics associated with test 6

The computed values of  $(E/t)$  on the landward grassed slope are very small and not shown in Figure 8. The computed erosion rate increases slightly with  $t$  because of the decrease of  $R$  in Equation 2 with the increase of  $E$  as shown in Figure 3. The measured average erosion rate was 3.3 mm/h for zone 1 between  $0.3 H_s$  to  $0.6 H_s$

below SWL and 1.5 mm/h for zone 2 between 0.0 to 0.3  $H_s$  below SWL where  $H_s = 1.4$  m for test 6. The measured average rates are indicated by the horizontal bars in zones 1 and 2. The measured erosion rate was indicated as 0 mm/h above SWL but no specific value was given in the zone lower than 0.6  $H_s$  below SWL. The crest and the zone of  $(-4.8 \text{ m}) < z < (-2.8 \text{ m})$  were constructed of concrete instead of the grass cover as illustrated in Figure 8. The numerical model roughly reproduces the measured erosion pattern. The location of the computed maximum erosion rate could be shifted seaward by increasing the breaking wave efficiency  $e_B = 0.0002$  in Equation 8 where  $e_B = 0.005$  for sand suspension. The large increase of  $e_B$  would cause too much erosion in the breaker zone. The low efficiency of breaking waves in eroding the grassed levee may be related to the intermittent nature of turbulence generated by breaking waves and the ductile nature of the grass cover resistance.

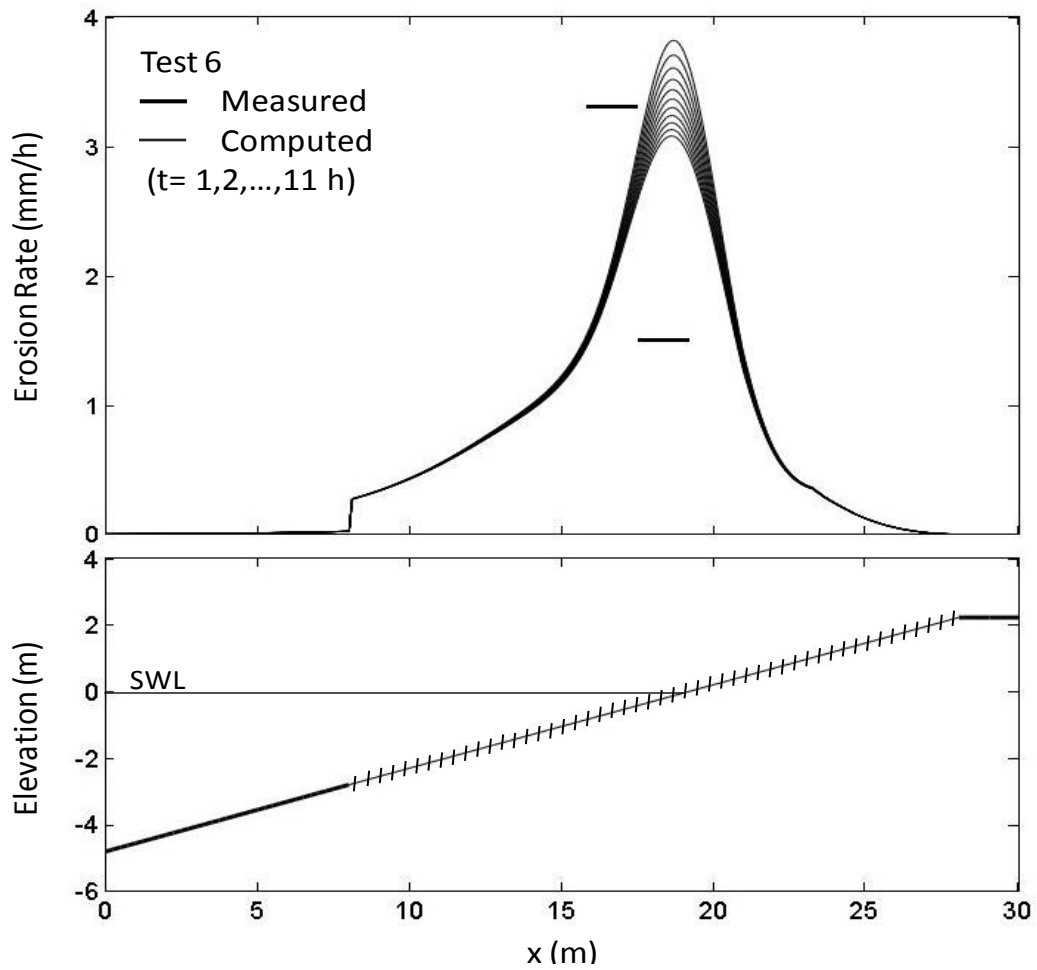


Figure 8 Measured and computed erosion rates on seaward grass cover for test 6

For test 7 with  $H_s = 0.75$  m, the grass cover inspection and profile survey were performed every 4 hours. The computed maximum erosion depth at  $t = 20$  h is less than 3 cm, shown in Figure 9.

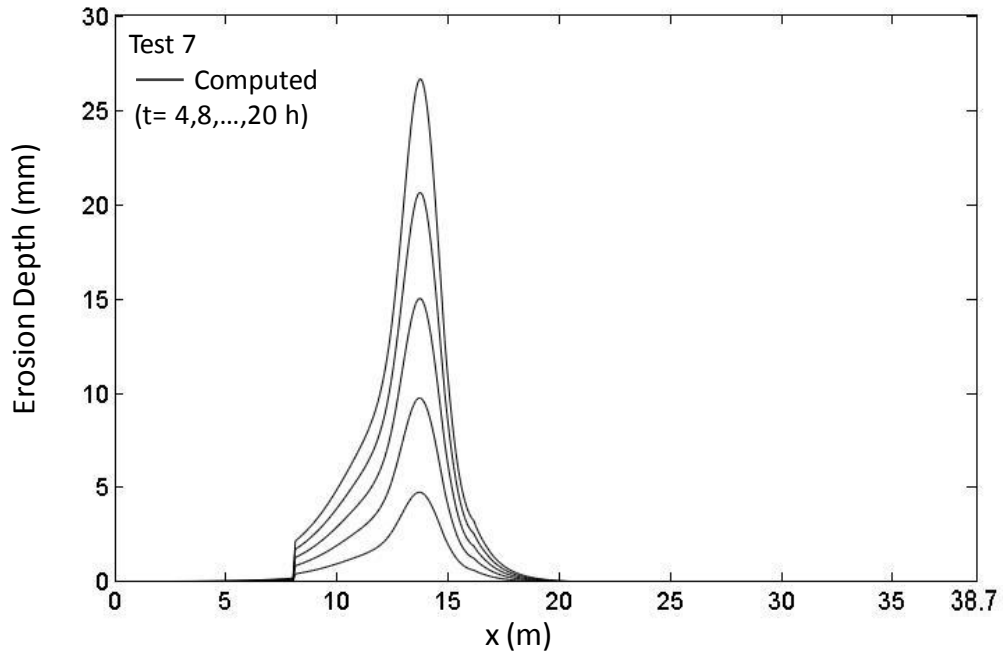


Figure 9 Computed erosion depth increase with time  $t$  for test 7

The computed cross-shore variations of  $\bar{\eta}$ ,  $\sigma_{\eta}$ ,  $\bar{U}$ ,  $\sigma_U$ , and  $P_w$  at  $t = 4, 8, \dots, 20$  h are almost identical and end well below the crest because of no wave overtopping, which is depicted in Figure 10.

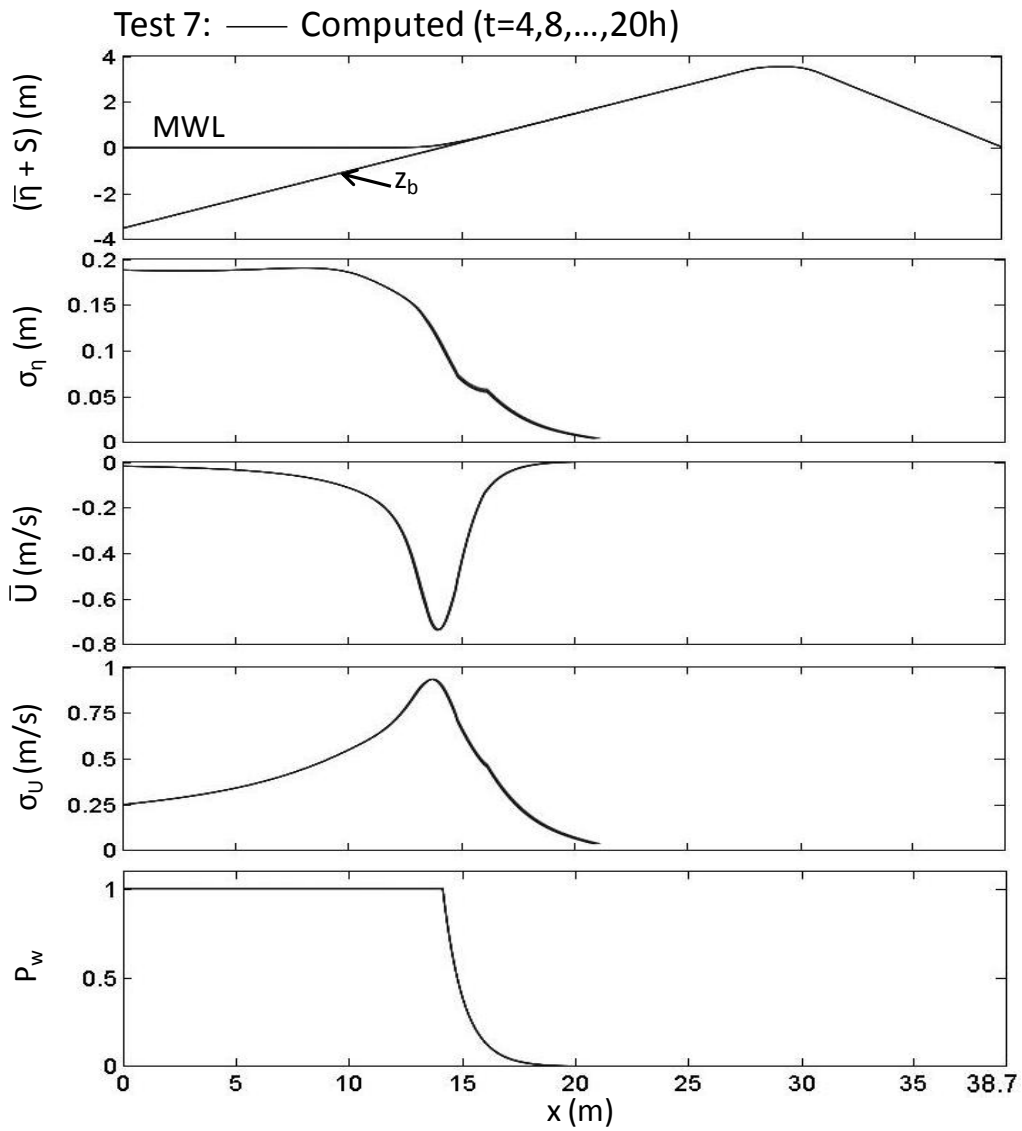


Figure 10 Computed hydrodynamics associated with test 7

The computed cross-shore variations of the erosion rate ( $E/t$ ) at  $t = 4, 8, \dots, 20$  h are shown along with experimental levee section in Figure 11. The measured average erosion rates of 1.0 mm/h in zone 1 and 0.5 mm/h in zone 2 are indicated by the horizontal bars in Figure 11. The reduced erosion rate is reproduced by the

numerical model but the maximum erosion rate is computed to occur too close to the still water shoreline as is the case in Figure 8.

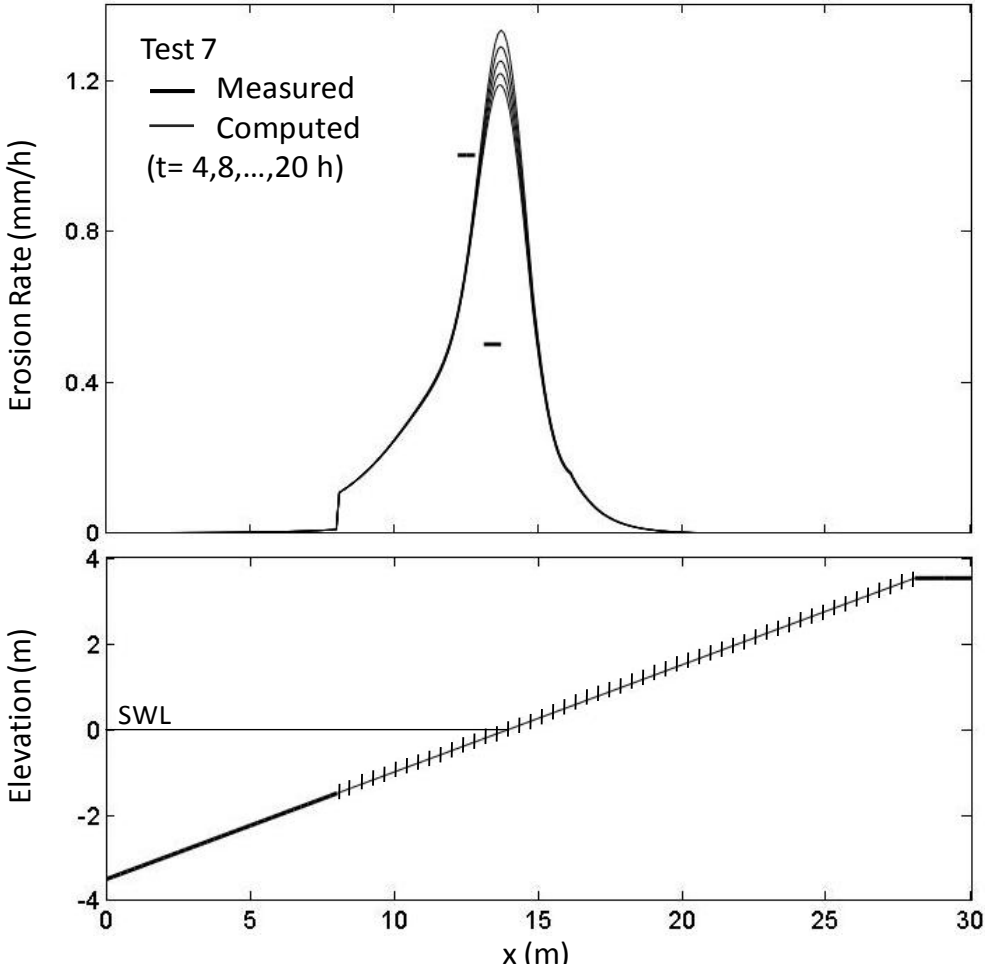


Figure 11 Measured and computed erosion rates on seaward grass cover for test 7

Smith et al. (1994) observed the development of a hole in test 6. The hole development was defined as the occurrence of local erosion progression through the root layer. The hole in test 6 occurred 1 m below SWL. The diameter and depth of

the hole were 0.75 m and 0.12 m at  $t = 9$  h, respectively, and increased to 1.0 m and 0.15 m at  $t = 11$  hr. No hole was observed in test 7. The present levee erosion model based on the assumption of alongshore uniformity cannot predict the development of a three-dimensional hole. Erosion of a strip of a poor grass cover is analyzed instead. The strip of cross-shore width of 1.2 m is assumed to be located in the zone of 1.0 to 1.3 m below SWL. The surface resistance parameter  $R_0$  is reduced to  $R_0 = 200 \text{ m}^2/\text{s}^2$  for the poor grass cover from  $R_0 = 1,000 \text{ m}^2/\text{s}^2$  for the good grass cover. Figure 12 shows the computed cross-shore variations of the erosion depth at  $t = 1, 2, \dots, 11$  h for test 6 H where the letter H indicates a two-dimensional hole. The strip of the poor grass cover on the levee section in Figure 12 corresponds to the 1.2-m wide zone between the good grass cover indicated by short vertical lines. The erosion depth  $E$  for the good grass cover increases slowly with time  $t$  and is less than 4 cm at  $t = 11$  hr. The computed value of  $E$  for the poor grass cover becomes larger than the grass cover thickness of  $d = 10$  cm at  $t = 9$  hr and increases rapidly during  $t = 9 - 11$  h. The computed erosion depth of  $E = 40$  cm at  $t = 11$  h is too large partly because the hydrodynamic model in CSHORE is too crude to predict the complicated flow above and inside the two-dimensional hole. The effects of the hole on the computed cross-shore variations of  $\bar{\eta}$ ,  $\sigma_\eta$ ,  $\bar{U}$ ,  $\sigma_U$ , and  $P_w$  are discernible and presented in Figure 13, but the depth-averaged velocity  $U$  does not represent the reduced velocity inside the deep hole. The present levee erosion model does not predict the increase of the hole width after the hole development, probably because lateral erosion underneath the grass cover is not included in the model.

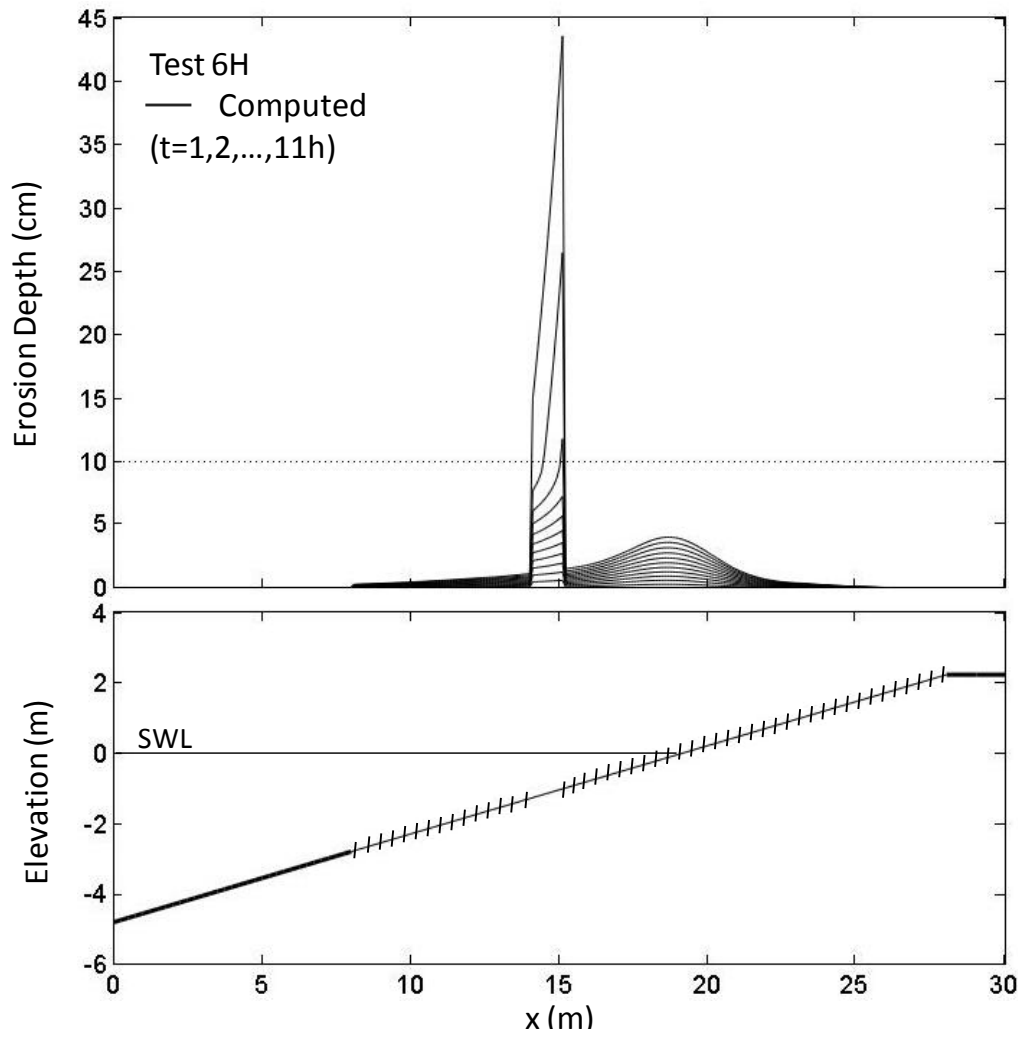


Figure 12 Computed erosion depth increase with time  $t$  for test 6H with poor grass patch

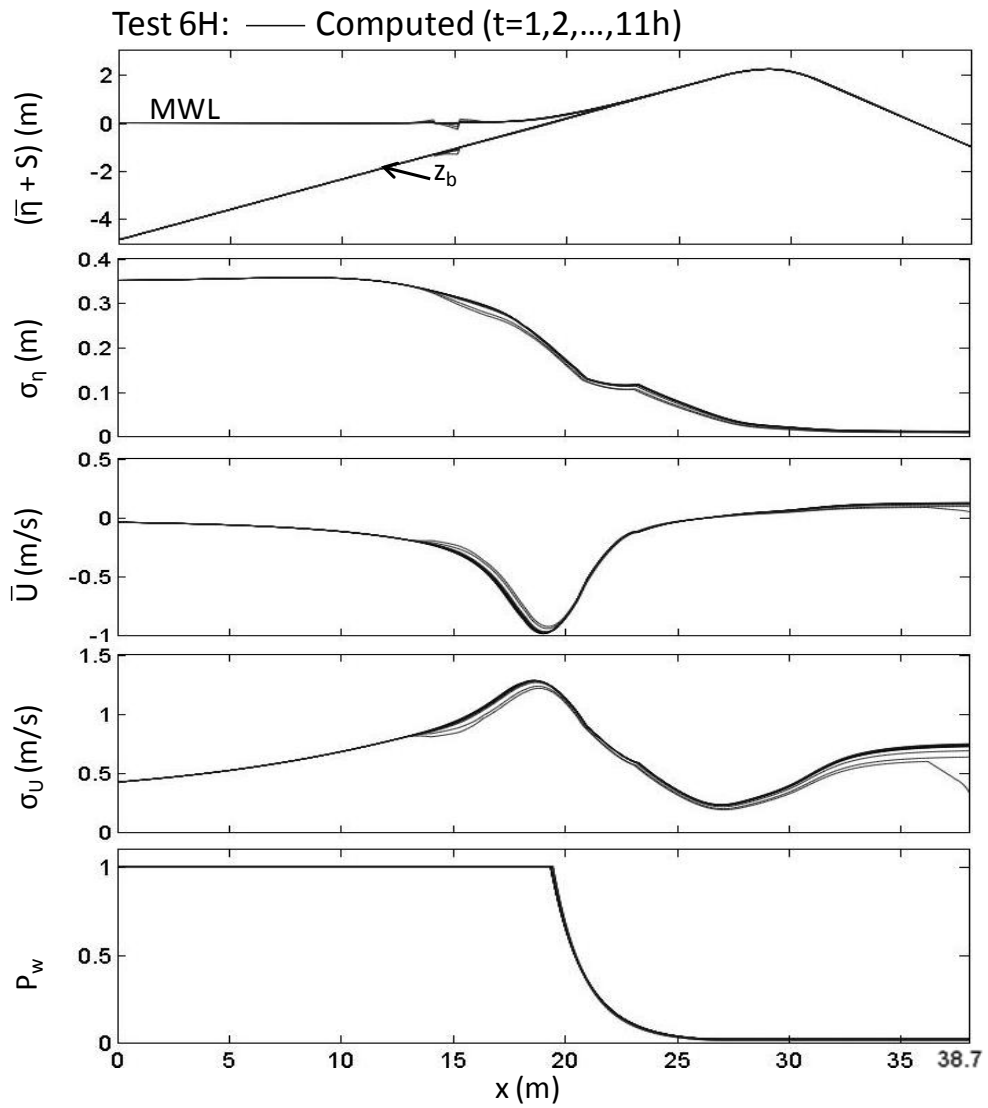


Figure 13 Computed hydrodynamics associated with test 6H

Figure 14 shows the computed cross-shore variations of the erosion depth at  $t = 4, 8, \dots, 20$  h for test 7H where the 1.2-m wide strip of the poor grass cover is located in the zone of 1.0 to 1.3 m below SWL on the levee section. The erosion depth  $E$  increases with time but the hole development defined as  $E > d$  through the

poor grass cover does not occur because  $E < 3$  cm at  $t = 20$  h. The computed cross-shore variations of  $\bar{\eta}$ ,  $\sigma_{\eta}$ ,  $\bar{U}$ ,  $\sigma_U$ , and  $P_w$  at  $t = 4, 8, \dots, 20$  h are shown in Figure 15 and are almost identical because of the negligible levee profile change. The energy dissipation rate  $D$  in Equation 2 changes little with  $t$  for test 7H. If  $E$  is small relative to  $d = 10$  cm, the erosion resistance  $R$  in Equation 2 can be approximated by  $R_0$ , and  $E$  is approximately proportional to  $R_0^{-1}$ . The reduction of  $R_0$  by a factor of 5 leads to the increase of  $E$  by a factor of about 5.

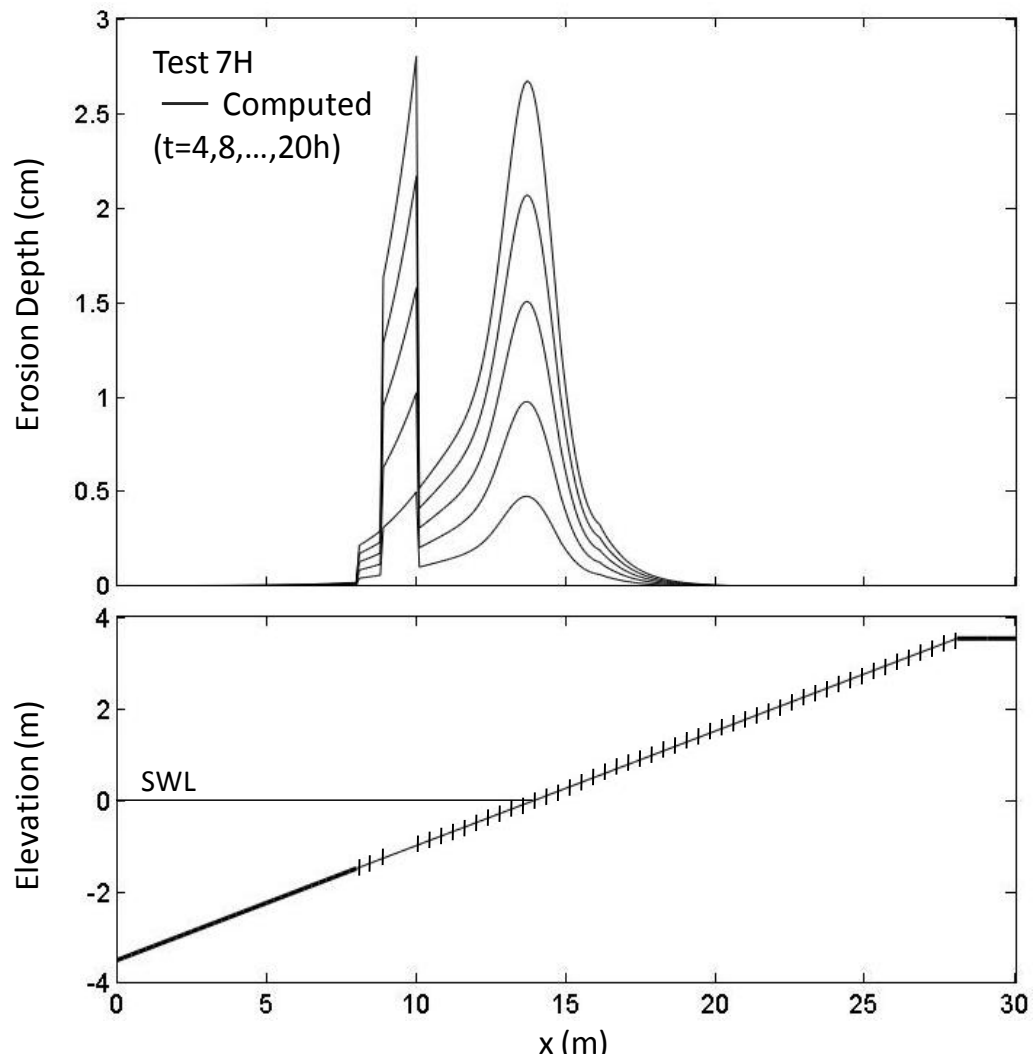


Figure 14 Computed erosion depth increase with time  $t$  for test 7H with poor grass patch

This proportionality and the approximate linear relation between  $E$  and  $t$  explain why  $E$  of the poor grass cover at  $t = 4$  h appears to be continuous with  $E$  of the good grass cover at  $t = 20$  h. Figure 14 implies that the accurate prediction of  $E$  requires the reliable quantification of  $R_0$ .

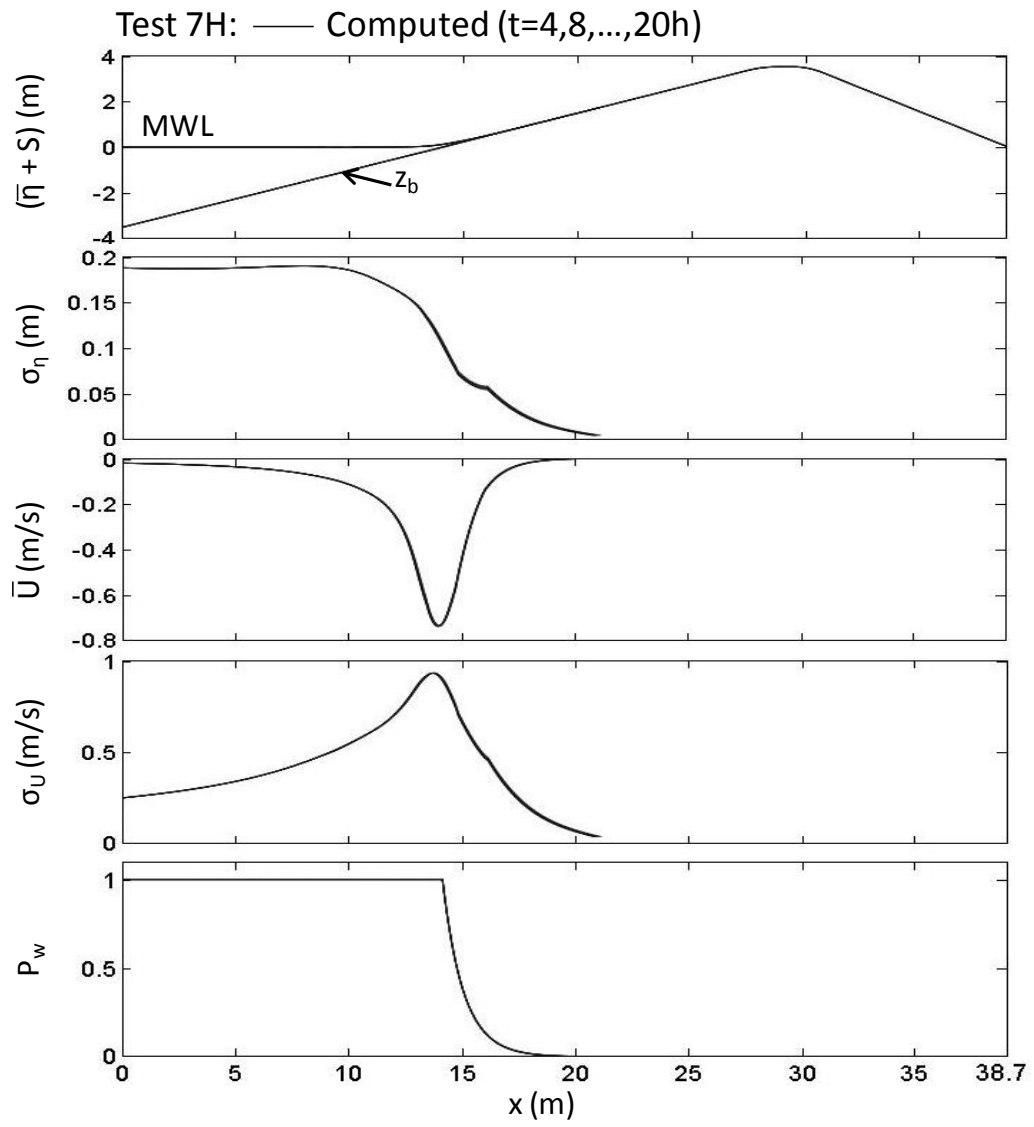


Figure 15 Computed hydrodynamics associated with test 7H

## Chapter 5

### EROSION OF SEAWARD CLAY SLOPE

Wolters et al. (2008) removed the top layer of 1-m thickness from an old levee in the Netherlands and excavated 36 boulder clay blocks. The length, width, and height of each block were 1.8 m, 1.3 m and 1.6 m, respectively. The blocks were transported to construct a seaward clay slope of a levee in a large wave flume. The slope was 1/3 and the levee crest height was 8.3 m above the horizontal flume bottom. The water depth at the toe of the levee was 4.5 m. The maximum clay layer thickness was 3 m on the 1/3 slope. The clay layer extended from 1.6 m below SWL to 2.4 m above SWL. The zones below and above the clay layer were constructed of compacted clay and concrete. The boulder clay was structured clay with a network of cracks formed under the long-term weathering and erodes much faster than unstructured clay (Klein Breteler et al. 2012). For the following computation,  $R_0 = 10,000 \text{ m}^2/\text{s}^2$  for the concrete and compacted clay is assumed to limit erosion to the clay layer with  $d = 0 \text{ m}$  and  $R_d = 10 \text{ m}^2/\text{s}^2$ . The erosion depth  $E$  is computed using Equation 6 with  $d = 0$  and  $t_d = 0$ . The wave conditions starting from  $t = 0$  were varied in six steps at  $t = 0.5, 1.31, 2.31, 3.55, 5.23,$  and  $5.98 \text{ h}$  (end of the last step). The spectral significant wave height  $H_{m0}$  was 1.12, 1.17, 1.51, 1.56, 1.58, and 1.57 m in the first to sixth steps. The corresponding peak period  $T_p$  was 4.97, 5.01, 5.73, 5.77, 5.72, and 5.98 s, respectively. The eroded clay profile was measured at the end of each step.

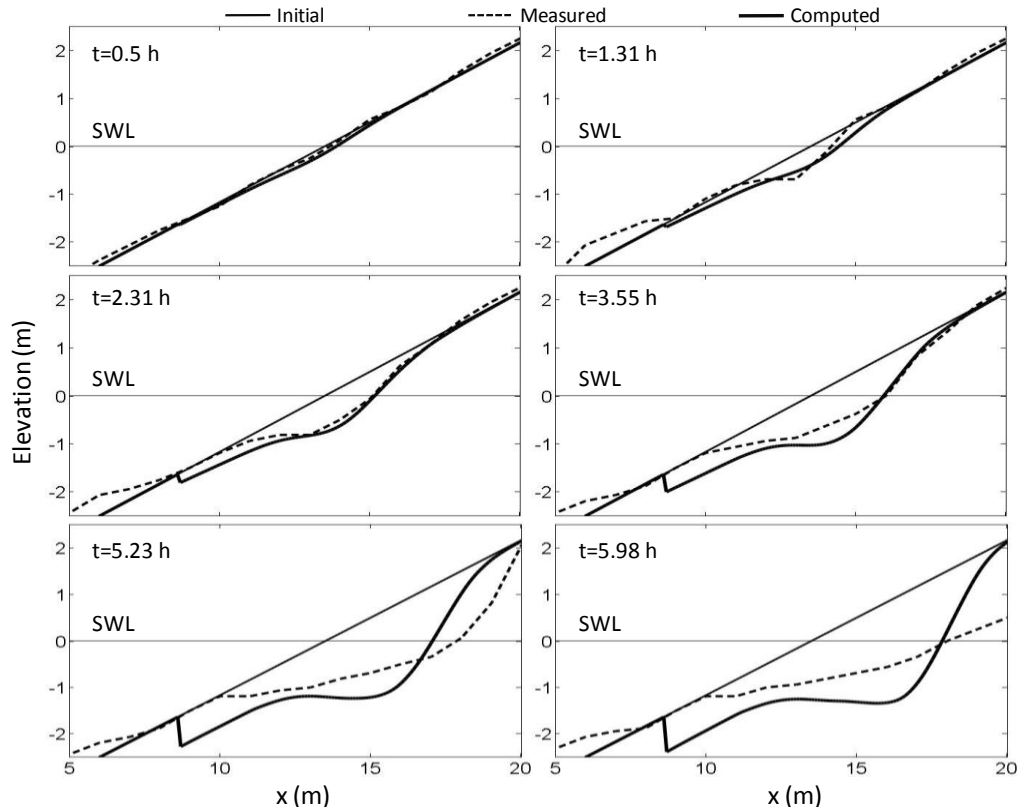


Figure 16 Measured and computed profile evolutions of seaward clay slope

Figure 16 compares the measured and computed profiles at  $t = 0.5, 1.31, 2.31, 3.55, 5.23,$  and  $5.98$  h. The downward erosion is predicted well at  $t = 0.5$  and  $1.31$  h but overpredicted near  $x = 8.7$  m at  $t = 2.31$  to  $5.98$  h where the boundary between the boulder clay and compacted clay was located at  $x = 8.7$  m. The overprediction may be related partly to the deposition of the eroded clay in the zone of  $x < 8.7$  m where the eroded clay is assumed to be transported seaward of the levee toe at  $x = 0$  in this levee erosion model. The computed erosion depth  $E$  is proportional to  $R_d^{-1}$  and can be decreased by reducing the breaking wave efficiency  $e_B = 0.0002$  in Equation 8. The adopted values of  $R_d$  and  $e_B$  are based on a number of computations made using the

different combinations of  $R_d$  and  $e_B$ . The large profile changes in Figure 16 modify the cross-shore variations of  $\bar{\eta}$ ,  $\sigma_\eta$ ,  $\bar{U}$ ,  $\sigma_U$ , and  $P_w$ . The hydrodynamic computations are interconnected with the erosion computations for this case and are presented in Figure 17.

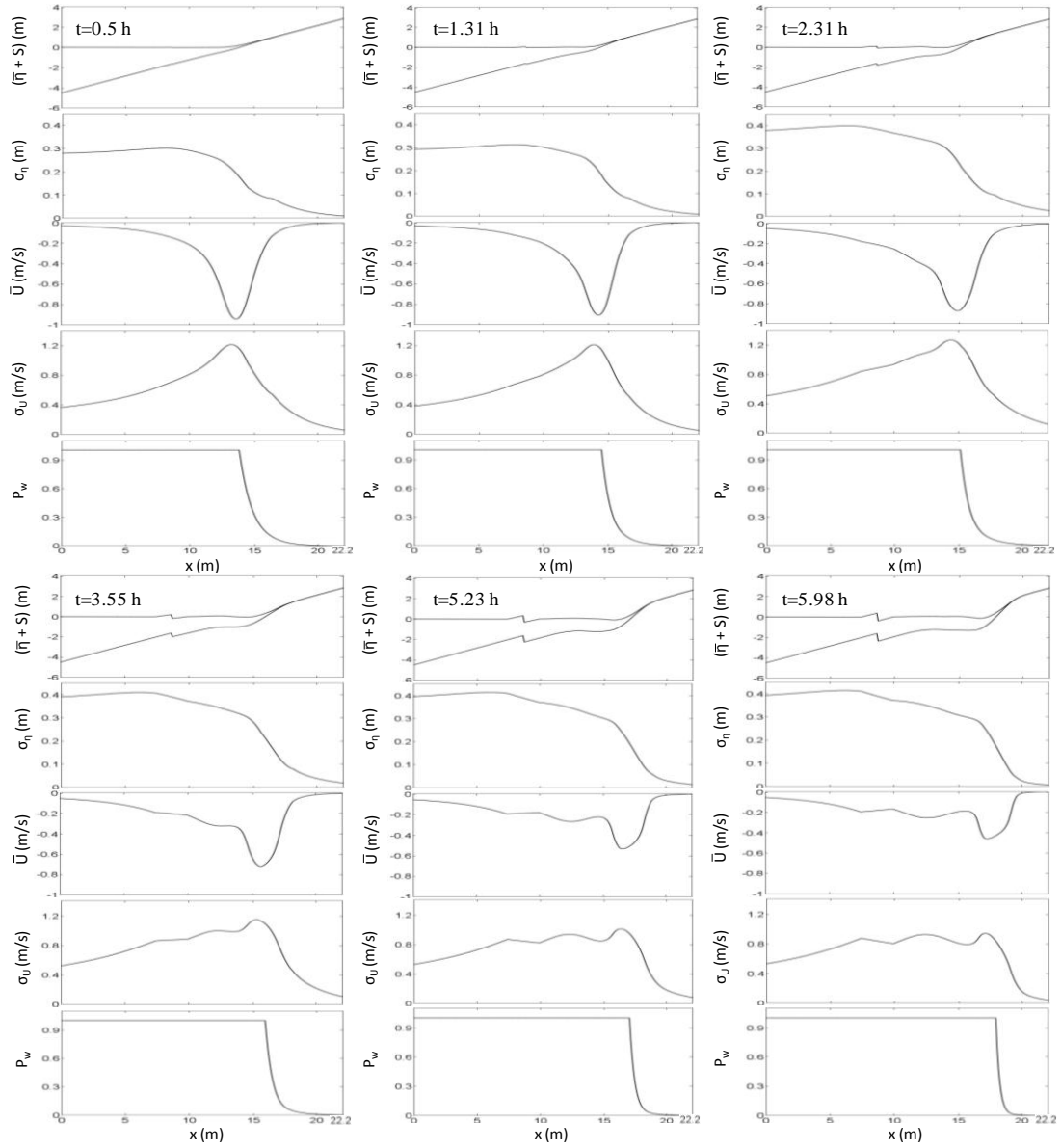


Figure 17 Computed hydrodynamics on seaward clay slope

On the other hand, the horizontal erosion of the eroded profile above SWL is predicted well at  $t = 0.5$  to  $3.55$  h but underpredicted at  $t = 5.23$  and  $5.98$  h. The

boundary between the boulder clay and compacted clay was located at  $x = 20.7$  m and the measured profile close to this boundary was not presented by Wolters et al. (2008).

The bottom slope function  $G_s$  given by Equation 9 is added to Equation 8 to better reproduce the horizontal erosion of the steep eroded profile above SWL. The calibrated limiting clay slope is  $S_c = 1.2$  in Equation 9 and  $G_s = 6$  for the steep bottom slope,  $S_b = 1.0$ , which was the approximate value given by Klein Breteler et al. (2012). Figure 18 compares the measured and computed eroded areas  $A_e$  as a function of  $t$  where  $A_e$  is defined as the area of the eroded profile at given  $t$  below the initial 1/3 slope. The computed values of  $A_e$  for  $S_c = 1.1, 1.2,$  and  $1.3$  are almost the same for  $t \leq 2.31$  h where  $S_b$  is relatively small. The adopted value of  $S_c = 1.2$  yields the best agreement for  $t \geq 3.55$  h.

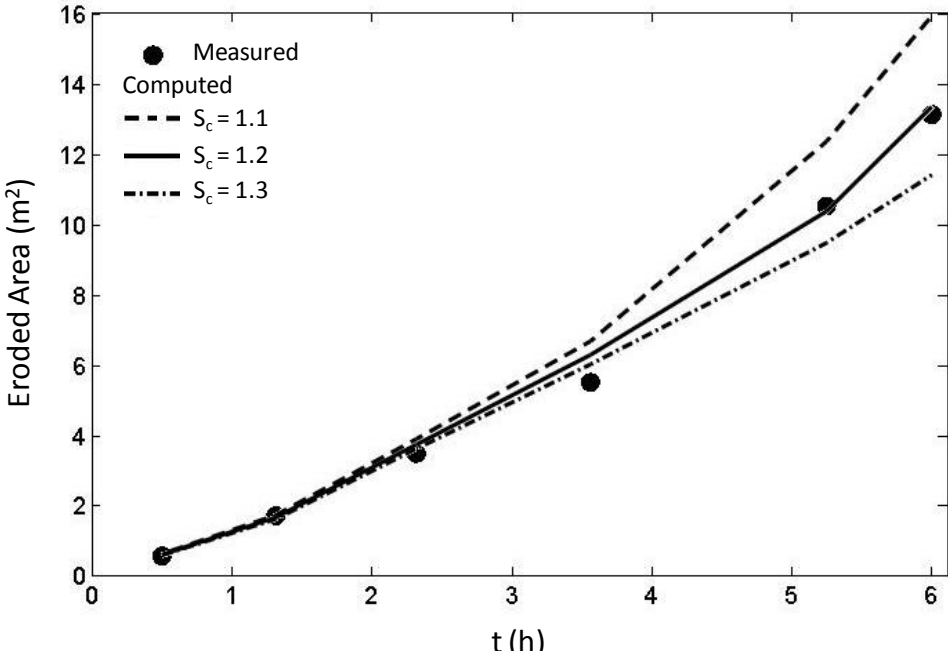


Figure 18 Increase of measured and computed eroded areas with time  $t$  for seaward clay slope

## Chapter 6

### EROSION OF LANDWARD GRASSED SLOPE

Steendam et al. (2010) performed a number of tests on real levees to examine the behavior of the grass cover on the landward slope. These tests were conducted on the good grass cover. The numerical model is compared with test V1 because the cross section of the landward slope and crest of the Vecht levee for test V1 was presented by Steendam et al. (2010). The Wave Overtopping Simulator (van der Meer et al. 2010) simulates the overtopping wave volumes at the crest of an actual levee. The overtopping volumes of irregular waves were calculated for the specified significant wave height  $H_s$  and peak period  $T_p$  at the toe of a seaward slope of 1/4. The cross section of the levee in Figure 1 is based on that of test V1. The crest height of the levee above the datum  $z = 0$  was 3.7 m and the crest width was 3m. The toe of the seaward 1/4 slope is assumed to be located at  $z = -5$  m so that the incident waves with  $H_s = 2$  m and  $T_p = 5.7$  s do not break seaward of the levee toe located at  $x = 0$ . The still water level  $S$  is chosen to produce the wave overtopping rate  $q_o$  on the crest specified for test V1. The hydrodynamic model in CSHORE for the fixed bottom is used to obtain the relation between  $S$  and  $q_o$ . The computed relation for  $H_s = 2$  m and  $T_p = 5.7$  s is shown in Figure 19. For  $H_s = 2$  m,  $q_o = 1 - 90 \ell/s/m$  for  $S = (-1.2) - 2.0$  m. The computed relation for  $H_s = 1$  m and  $T_p = 4.0$  s is also presented because van der Meer et al. (2010) examined the difference of individual wave overtopping volumes caused by the wave height difference for the same value of  $q_o$ . For  $H_s = 1$  m,  $q_o = 1 - 90 \ell/s/m$  for  $S = 1.8 - 3.4$  m where  $S = 3.7$  m corresponds to

the levee crest elevation. The rate  $q_o$  increases more rapidly with the increase of  $S$  for  $H_s = 1$  m than  $H_s = 2$  m.

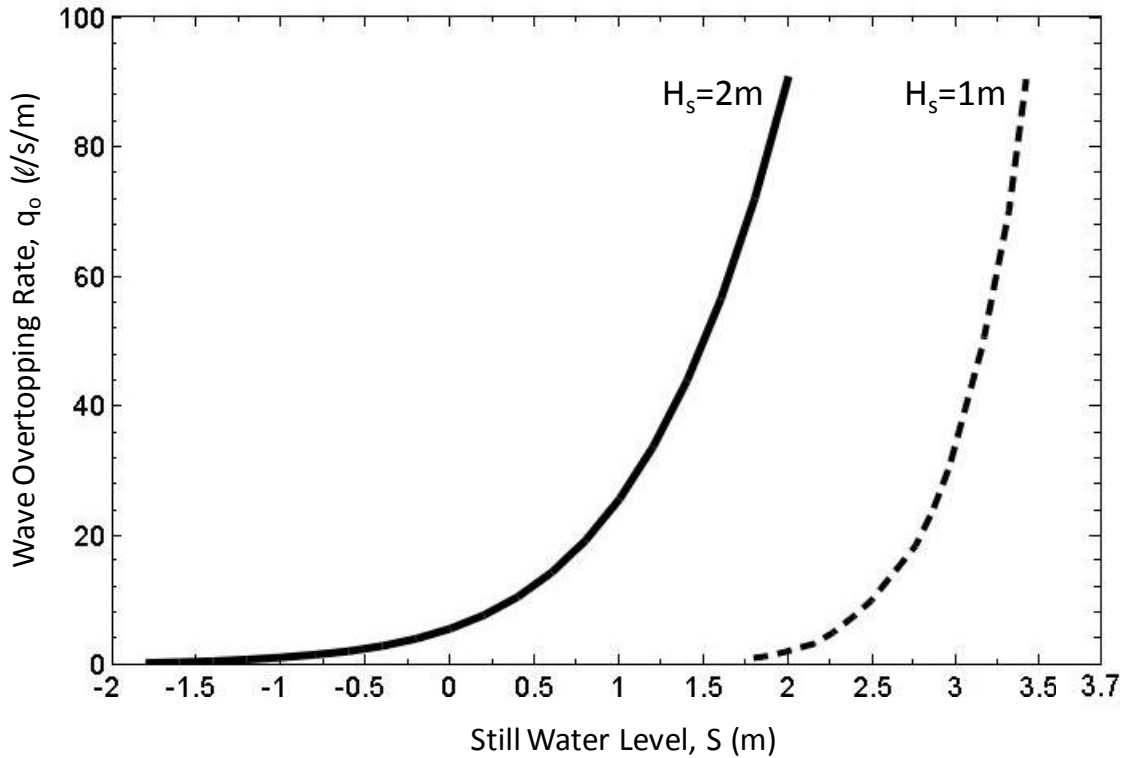


Figure 19 Increase of computed wave overtopping rate  $q_o$  with still water level  $S$  for test VI

The landward slope of test V1 is depicted in the bottom panel of Figure 20. A maintenance road was located in the middle of the slope. The grassed zones above and below the road are indicated by short vertical lines in Figure 20. The road consisted of bricks that allowed grass growth. The landward slope was subjected to the sequence of  $q_o = 1, 10, 30$  and  $50 \ell/s/m$  based on  $H_s = 2$  m. The duration of each value of  $q_o$  was 6 hours. Initial damage developed at the seaward edge of the

maintenance road during  $q_o = 1 \ell/s/m$ . The initial damage progressed slowly during  $q_o = 10 \ell/s/m$  and evolved into two substantial holes undermining the road during  $q_o = 30 \ell/s/m$ . At the beginning of  $q_o = 50 \ell/s/m$ , some bricks were dislodged and some of the grass cover was eroded from the toe and berm in the zone of  $x = 48 - 50$  m in Figure 20.

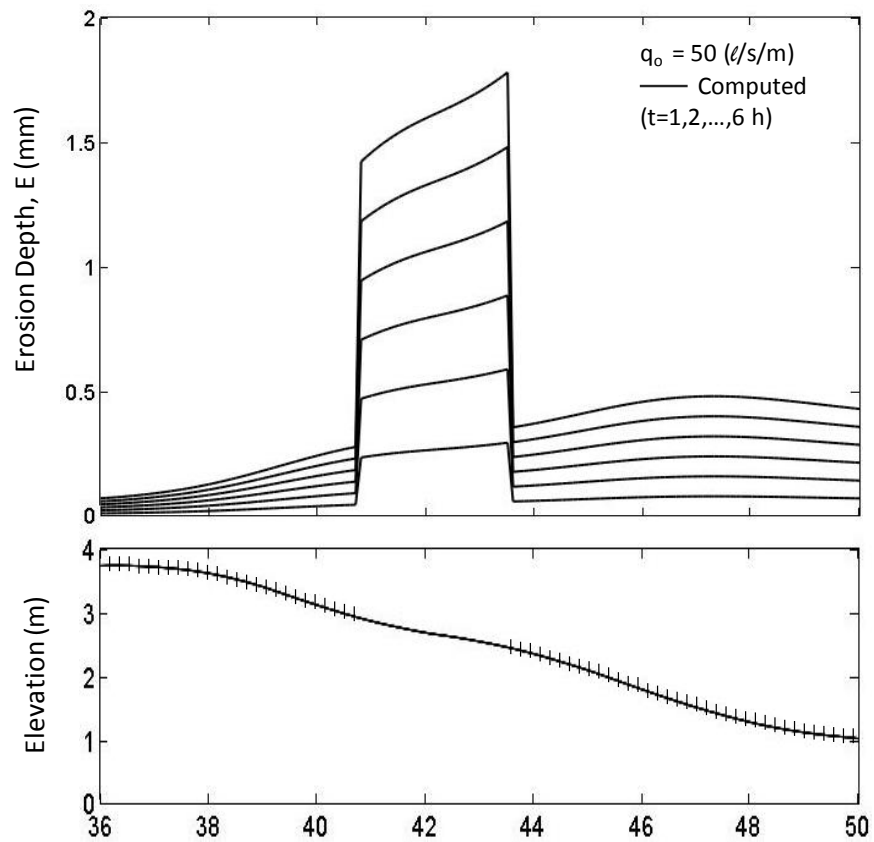


Figure 20 Computed erosion depth increase with time  $t$  for test VI with poor grass patch

The numerical model cannot simulate the observed damage progression in test V1 partly because local flow disturbance and damage initiation are not taken into account. Figure 20 shows the computed erosion depth  $E$  on the landward slope at  $t = 1, 2, \dots, 6$  h for  $q_o = 50 \ell/s/m$  where  $E = 0$  at  $t = 0$ . The maintenance road is crudely represented as a strip of a poor grass cover with  $R_0 = 200 \text{ m}^2/s^2$  where  $R_0 = 1,000 \text{ m}^2/s^2$  for the good grass cover. The computed  $E$  of the poor grass cover at  $t = 1$  h is almost continuous with that of the good grass cover at  $t = 5$  h because  $E$  is approximately proportional to  $R_0^{-1}$  and  $t$  for the small erosion of 2 mm or less. The numerical model predicts the downward increase of  $E$  on the inclined slope but the predicted value of  $E$  is too small.

The sensitivity of  $E$  to  $q_o$  in the range of  $q_o = 1 - 90 \ell/s/m$  is examined by computing the cross-shore variation of  $E$  on the landward slope of the same profile but covered with only the good grass cover. The maximum value of  $E$  occurs near the toe of the landward slope. The maximum erosion depth  $E_{\max}$  increases with the increase of  $t$  and  $q_o$  but  $E_{\max}$  is about 1 mm at  $t = 6$  h for  $q_o = 90 \ell/s/m$ , depicted in Figure 21.

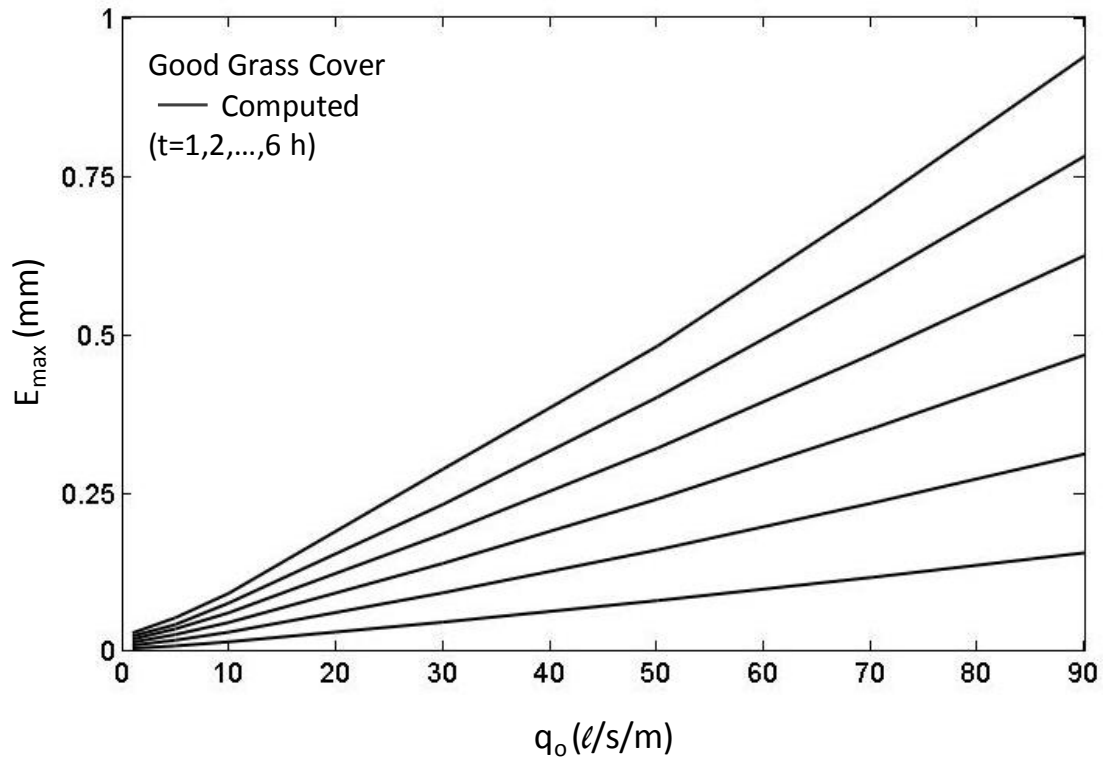


Figure 21 Computed maximum erosion depth  $E_{\max}$  at slope transition of good grass cover as a function of  $q_o$  and  $t$

For the poor grass cover,  $E_{\max}$  is about 5 mm at  $t = 6$  h for  $q_o = 90 \ell/s/m$  as shown in Figure 22. Figure 23 shows the computed  $E_{\max}$  at  $t = 1, 2, \dots, 6$  h as a function of  $q_o$  for the landward clay slope with  $R_0 = R_d = 10 \text{ m}^2/s^2$ . For the clay slope,  $E_{\max}$  is about 10 cm at  $t = 6$  h for  $q_o = 90 \ell/s/m$ . The surface resistance parameter  $R_0$  determines the degree of erosion on the landward slope. The wave overtopping rate  $q_o$  and duration  $t$  are also important but more predictable than the uncertain parameter  $R_0$ . The computed difference between  $H_s = 2$  m and 1 m is found to be small and  $q_o$  may be used to represent the erosion work by overtopping waves.

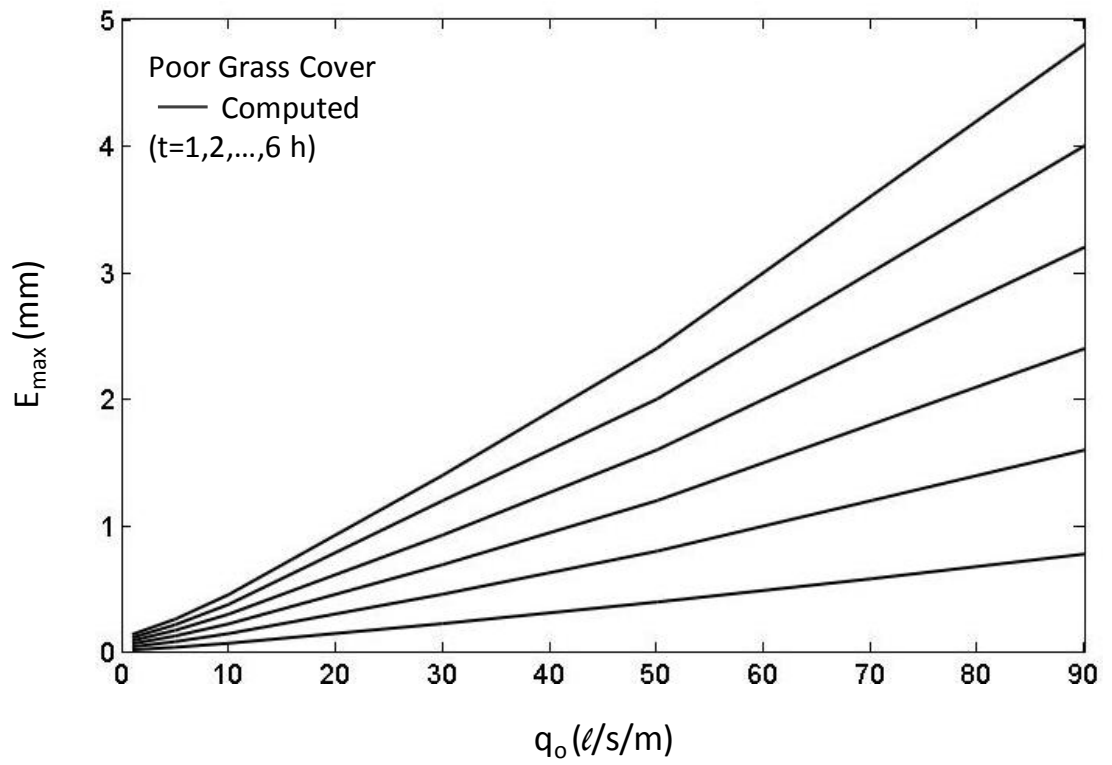


Figure 22 Computed maximum erosion depth  $E_{max}$  at slope transition of poor grass cover as a function of  $q_0$  and  $t$

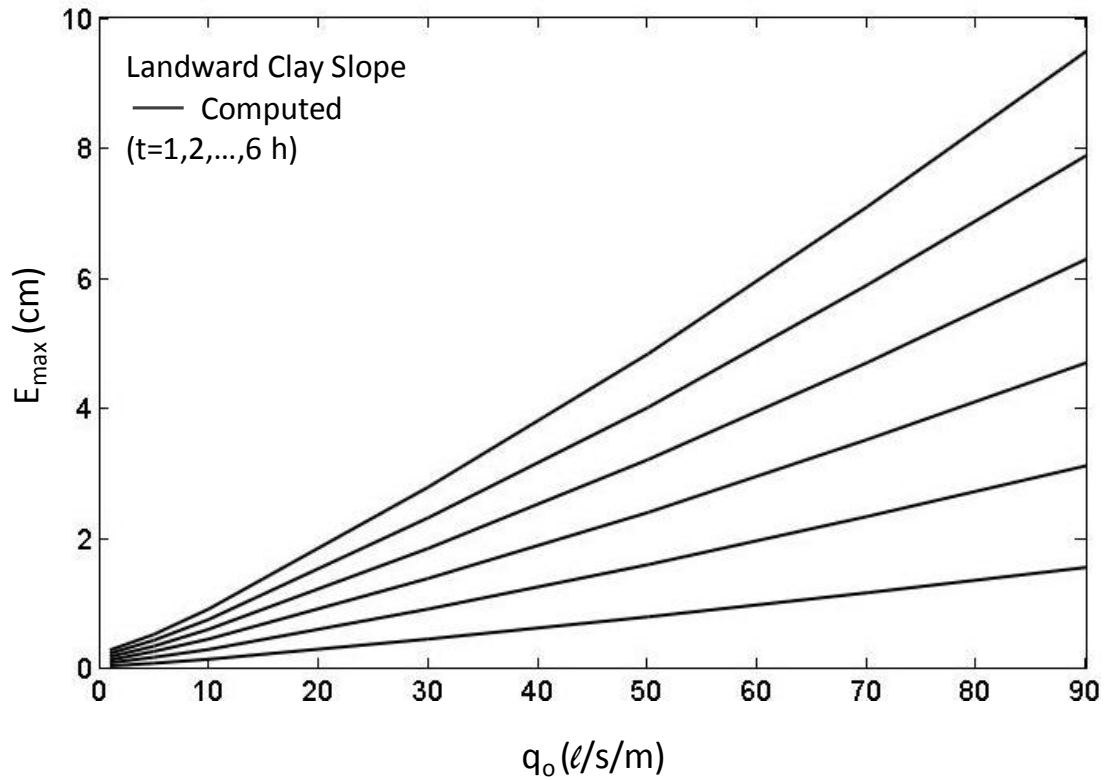


Figure 23 Computed maximum erosion depth  $E_{\max}$  at slope transition of landward clay slope as a function of  $q_o$  and  $t$

The computed results presented in these figures are discussed in light of other available data. Thornton et al. (2011) examined resiliency of different landward slope surfaces using a large-scale wave overtopping test facility. The levee geometry consisted of a downward 1/3 slope with a height of 2.7 m that transitioned to a 3.6-m long berm on a 1/25 slope. This geometry is similar to that shown in Figure 20. Bermuda grass in planter trays was cultivated and well maintained for 6 months prior to testing. This grass cover with dense roots, ample thatching, and few imperfections suffered little damage under the 24-hour incremental increase of  $q_o$  up to 370  $\ell$ /s/m. The Bahia grass cover suffered little damage under the 17-hour incremental increase

of  $q_o$  up to 279  $\ell/s/m$ . The grass cover model in Figure 3 with  $R_0 = 200 - 1,000$   $m^2/s^2$ ,  $d = 0.1$  m, and  $R_d = 10$   $m^2/s^2$  appears to correspond to the nearly perfect grass cover with few imperfections. The previously tested Bermuda grass went dormant during winter. The dormant Bermuda grass was tested in sequence of  $q_o = 186, 232$  and 186  $\ell/s/m$  with a 1-hour interval. Minor erosion evolved into a 2.7-m long trench with a cross-flume width of 15-30 cm and a depth of 5-15 cm. This trench development is somewhat similar to the hole development discussed in relation to Figures 12 and 14. Thornton et al. (2011) also tested a bare clay surface. Significant soil loss occurred in one hour under  $q_o = 9.3$   $\ell/s/m$ . The bare clay test was continued under  $q_o = 18.6$   $\ell/s/m$  but suspended after 20 min because the clay slope failed catastrophically. The computed erosion depths for the clay slope in Figure 23 indicate  $E_{max} < 1$  cm for  $t < 2$  h and  $q_o < 20$   $\ell/s/m$ . The clay erosion could be increased by reducing  $R_0 = R_d = 10$   $m^2/s^2$  but Thornton et al. (2011) did not describe the clay characteristics.

Steendam et al. (2012) conducted wave overtopping tests on a real levee with a poorly-maintained grass cover in contrast to the good grass cover tests by Steendam et al. (2010). The bad grass cover with holes made by moles had no resistance against overtopping waves. They concluded that a bad grass cover should be considered as an unprotected clay layer. The wave overtopping tests on real levees indicate the wide variations of grass covers. The simple grass cover model in Figure 3 may become more realistic if the spatial variations of  $R_0$ ,  $R_d$  and  $d$  are known because damage tends to initiate from weak spots.

## **Chapter 7**

### **SUMMARY AND CONCLUSIONS**

A levee erosion model is developed to predict the temporal and cross-shore variations of vertical erosion depth under irregular wave action. The product of the erosion rate and the turf resistance force is related to the wave energy dissipation rates due to wave breaking and bottom friction. The dissipation rates are computed using the hydrodynamic model in the cross-shore numerical model CSHORE. The turf resistance force is characterized by the turf thickness and the surface and underneath resistance parameters. The empirical parameters in the erosion model are calibrated using available data. The relation between the limiting velocity and steady flow duration is used to estimate the order of magnitude of the surface resistance parameter. Large-scale erosion tests for seaward grassed and clay slopes are used to estimate the underneath resistance parameter, the breaking wave efficiency, and the limiting clay slope. Breaking waves are found to be much less efficient in eroding the cohesive levee than in suspending sand particles on beaches. The calibrated erosion model is shown to reproduce the erosion rate on the grassed slope and the eroded clay profile evolution. The levee erosion model is also compared with field and large-scale laboratory tests for erosion on the landward slope caused by wave overtopping. The comparisons indicate the difficulty in reproducing the observed erosion initiation and progression partly because of the wide variations of the grass cover and clay resistance. For practical applications, the turf resistance parameters in the model will need to be calibrated for specific levees.

Alongshore variability will need to be taken into account to make the model prediction more realistic. Wave-induced flow in small water depth is affected by the surface irregularity and initial erosion tends to occur on weak spots. The concentration of the flow on the eroded spots initiates the development of a hole or gully. The flow over the hole or gully becomes three-dimensional and the erosion progresses both vertically and laterally. Consequently, it is very challenging to develop a realistic erosion model even if the spatial variation of the grass cover resistance is known. A sensor will need to be developed to measure the spatial distribution of the turf resistance without damaging the levee. The accuracy of a levee erosion model depends on the reliable quantification of the turf resistance.

## REFERENCES

- Dean, R.G., Rosati, J.D., Walton, T.L., and Edge, B.L. (2010). "Erosional equivalences of levees: Steady and intermittent wave overtopping." *Ocean Eng.*, 37, 104-113.
- Dean, R.G., and van Ledden, M. (2010). "Accounting for levee overtopping duration: A test with Hurricane Katrina conditions." *Proc. 32nd Coastal Engineering Conf., Structures 1*, 1-15. <http://journals.tdl.org/ICCE/>
- Hewlett, H.W.M., Boorman, L.A., and Bramley, M.E. (1987). "Design of reinforced grass waterways." CIRIA Report 116, Construction and Industry Research and Information Association, London.
- Hoffmans, G., Akkerman, G.J., Verheij, H., van Hoven, A., and van der Meer, J. (2008). "The erodibility of grassed inner levee slopes against wave overtopping." *Proc. 31st Coastal Engineering Conf., World Scientific, Singapore*, 3224-3236.
- Klein Breteler, M., Bottema, M., Kruse, G.A.M., Mourik, G.C., and Capel, A. (2012). "Resilience of levees after initial damage by wave attack." *Proc. 33rd Coastal Engineering Conf., Structures 36*, 1-14. <http://journals.tdl.org/ICCE/>
- Kobayashi, N., Buck, M., Payo, A., and Johnson, B.D. (2009). "Berm and dune erosion during a storm." *J. Waterway, Port, Coastal, Ocean Eng.*, 135(1), 1-10.
- Kobayashi, N., Farhadzadeh, A., and Melby, J.A. (2010a). "Wave overtopping and damage progression of stone armor layer." *J. Waterway, Port, Coastal, Ocean Eng.*, 136(5), 257-265.
- Kobayashi, N., Farhadzadeh, A., Melby, J., Johnson, B., and Gravens, M. (2010b). "Wave overtopping of levees and overwash of dunes." *J. Coastal Res.*, 26(5), 888-900.
- Kobayashi, N., Payo, A., and Schmied, L. (2008). "Cross-shore suspended sand and bed load transport on beaches." *J. Geophys. Res.*, 113, C07001, 1-17.
- Kobayashi, N., Pietropaolo, J.A., and Melby, J.A. (2013). "Wave transformation and runup on levees and gentle slopes." *J. Coastal Res.*, 29(3), 615-623.

- Muijs, J.A., 1999. Grass cover as a dike revetment, Translation of TAWbrochure "Grasmat als Dijkbekleding", Rijkswaterstaat, Delft.
- Smith, G.M., Seijffert, J.W.W., and van der Meer, J.W. (1994). "Erosion and overtopping of a grass levee: Large scale model tests." Proc. 24th Coastal Engineering Conf., ASCE, Reston, Va., 2639-2652.
- Steendam, G.J., Provoost, Y., and van der Meer, J. (2012). "Destructive wave overtopping and wave run-up tests on grass covered slopes of real levees." Proc. 33rd Coastal Engineering Conf., Structures 64, 1-14.  
<http://journals.tdl.org/ICCE/>
- Steendam, G.J., van der Meer, J., Hardeman, B., and van Hoven, A. (2010). "Destructive wave overtopping tests on grass covered landward slopes of levees and transitions to berms." Proc. 32nd Coastal Engineering Conf., Structures 8, 1-14. <http://journals.tdl.org/ICCE/>
- Thornton, C., van der Meer, J., Scholl, B., Hughes, S., and Abt, S. (2011). "Testing levee slope resiliency at the new Colorado State University wave overtopping test facility." Proc. Coastal Structures 2011, World Scientific, Singapore, 167-178.
- van der Meer, J., Hardeman, B., Steendam, G.J., Schüttrumpf, H., and Verheij, H. (2010). "Flow depths and velocities at crest and landward slope of a levee, in theory and with the wave overtopping simulator." Proc. 32nd Coastal Engineering Conf., Structures 10, 1-15. <http://journals.tdl.org/ICCE/>
- van Gent, M.R.A. (2002). "Low-exceedance wave overtopping events: Measurements of velocities and the thickness of water-layers on the crest and inner slope of levees." Delft Cluster Rep. No. DC030202/H3802, Delft Hydraulics, Delft, The Netherlands.
- Wolters, G., Nieuwenhuis, J.W., van der Meer, J., and Klein Breteler, M. (2008). "Large scale tests of boulder clay erosion at the Wieringermeer levee (Ijsselmeer)." Proc. 31st Coastal Engineering Conf., World Scientific, Singapore, 3263-3275.
- Young, M.J., and Hassan, R.M. (2006). "Grass cover layer failure on the inner slope of levees." Proc. 30th Coastal Engineering Conf., World Scientific, Singapore, 2857-2869.